Lipopolysaccharide-induced alteration of mitochondrial morphology induces a metabolic shift in microglia modulating the inflammatory response *in vitro* and *in vivo*

Journal:	*GLIA*
Manuscript ID	GLIA-00368-2018.R1
Wiley - Manuscript type:	Original Research Article
Date Submitted by the Author:	n/a
Complete List of Authors:	Nair, Syam; Goteborgs Universitet Sobotka, Kristina; Goteborgs Universitet Joshi, Pooja; Université Paris Diderot gressens, Pierre; Université Paris Diderot; King's College London Fleiss, Bobbi; RMIT; King's College London; Université Paris Diderot Thornton, Claire; King's College London Mallard, Carina; Goteborgs Universitet Hagberg, Henrik; Goteborgs Universitet; King's College London
Key Words:	mitochondria, microglia, inflammation, metabolism, mitochondrial fission

Lipopolysaccharide-induced alteration of mitochondrial morphology induces a metabolic shift in microglia modulating the inflammatory response *in vitro* and *in vivo*

Syam Nair[1,2] , Kristina S. Sobotka[1,2], Pooja Joshi[3], Pierre Gressens[3,4], Bobbi Fleiss[3-5], Claire Thornton[4], Carina Mallard[1,2], Henrik Hagberg[1,4,6]

[1]Centre of Perinatal Medicine and Health, The Sahlgrenska Academy, University of Gothenburg, Gothenburg, Sweden;

[2]Institute of Neuroscience and Physiology, The Sahlgrenska Academy, University of Gothenburg, Gothenburg, Sweden;

[3]PROTECT, INSERM, Université Paris Diderot, Sorbonne Paris Cité, F-75019 Paris, France.

[4] Centre for the Developing Brain, Department of Division of Imaging Sciences and Biomedical Engineering, King's College London, King's Health Partners, St. Thomas' Hospital, London, SE1 7EH, United Kingdom;

[5]School of Health and Biomedical Sciences, RMIT University, Bundoora, VIC, Australia;

[6]Institute of Clinical Sciences, The Sahlgrenska Academy, University of Gothenburg, Gothenburg, Sweden.

Running title: LPS induced morphological and metabolic changes in microglia cells.

Acknowledgements.

We gratefully acknowledge the support from ERA-net (EU;VR 529-2014-7551), Wellcome Trust (WT094823), the Medical Research Council, Swedish Medical Research Council (VR 2015-02493, HH; VR 2012-2992, CM), Brain Foundation (HH, CM), Ahlen Foundation (HH, CM, SN), ALF-GBG (426401, HH; 432291, CM), and the Leducq Foundation (DSRRP34404), Torsten Söderberg (M98/15, CM), Frimurare Barnhusdirektionen (SN), to enable this study to be completed. In addition, the authors acknowledge financial support from the Department of Health via the National Institute for Health Research (NIHR) comprehensive Biomedical Research Centre Award to Guy's & St Thomas' NHS Foundation Trust in partnership with King's College London and King's College Hospital NHS Foundation Trust. Centre for Cellular Imaging at the University of Gothenburg and the National Microscopy Infrastructure, NMI (VR-RFI 2016-00968) for providing assistance in microscopy.

Corresponding author:

Henrik Hagberg, Department of Obstetrics and Gynecology,
Institute of Clinical Sciences, Journalvägen 6, 41685 Göteborg,
Email: henrik.hagberg@gu.se

Number of pages: 26, Number of figures: 9.

Word count

Abstract: 182, Introduction: 732, Materials and methods : 2331, Results:1405,
Discussion: 1507, Total word count: 6205

Conflict of interest: We report no conflict of interest

Abstract

Accumulating evidence suggests that changes in the metabolic signature of microglia underlie their response to inflammation. We sought to increase our knowledge of how pro-inflammatory stimuli induce metabolic changes. Primary microglia exposed to LPS expressed excessive fission leading to more fragmented mitochondria than tubular mitochondria. LPS mediated TLR4 activation also resulted in metabolic reprogramming from oxidative phosphorylation to glycolysis. Blockade of mitochondrial fission by Mdivi-1, a putative mitochondrial division inhibitor led to the reversal of the metabolic shift. Mdivi-1 treatment also normalized the changes caused by LPS exposure, namely an increase in mitochondrial ROS production and mitochondrial membrane potential as well as accumulation of key metabolic intermediate of TCA cycle succinate. Moreover, Mdvi-1 treatment substantially reduced LPS induced cytokine and chemokine production. Finally, we showed that Mdivi-1 treatment attenuated expression of genes related to cytotoxic, repair and immunomodulatory microglia phenotypes in an in vivo neuroinflammation paradigm. Collectively, our data show that the activation of microglia to a classically pro-inflammatory state associated with a switch to glycolysis that is mediated by mitochondrial fission, a process which may be a pharmacological target for immunomodulation.

Key words: inflammation, mitochondria, microglia, metabolism, mitochondrial fission

Main points:

LPS induces mitochondrial fragmentation and a metabolic switch in microglia. Blockade of fragmentation by Mdivi-1 reverses the metabolic shift, enhanced cytokine production, succinate accumulation *in vitro* and microglial activation *in vivo*.

Introduction

Microglia contribute to normal brain development, homeostasis and respond to pathological conditions by changing their phenotype from surveillance to pro-inflammatory, repair, regenerative and immunomodulatory states (Greter, Lelios, & Croxford, 2015; Tay, Savage, Hui, Bisht, & Tremblay, 2017). Studies of adult and neonatal injury and disease have conclusively shown that changes in the phenotype of microglia play a role in almost all forms of neuropathology (Solito & Sastre, 2012). Transcriptome analysis of microglia exposed to inflammatory stimuli revealed transient upregulation of important and stimulus-specific metabolic pathways (Thion et al., 2018), strongly suggesting that energy metabolism is modulated during brain inflammation. Microglia activation in response to stimuli that includes pathogen associated proteins, such as lipopolysaccharide (LPS), is a metabolically energy expensive event (Moss & Bates, 2001).

Mitochondria, which play a central role in energy metabolism, are dynamic organelles that undergo biogenesis, fission, fusion and mitophagy (autophagic degradation). The balance of these processes allows the reorganization of mitochondrial components and the elimination of damaged material, thereby maintaining a healthy mitochondrial population (Pickles, Vigie, & Youle, 2018; Wai & Langer, 2016) . Recent studies have linked mitochondrial dynamics to energy demand, suggesting changes in mitochondrial architecture as a mechanism for bioenergetic adaptation to inflammation (Nasrallah &

Horvath, 2014). By favoring either elongated or fragmented structures, mitochondria can regulate bioenergetic ability and thereby cell fate through metabolic programming (Buck et al., 2016). Although mitochondrial morphological changes are observed in response to alterations in oxidative metabolism (Hackenbrock, 1966), little is known of its role in microglia activation.

Microglia generate energy via both oxidative phosphorylation (OXPHOS) and glycolysis (Orihuela, McPherson, & Harry, 2016). OXPHOS occurs within the mitochondria and is more efficient for ATP synthesis in comparison to glycolysis. However, the preferential use of glycolysis over OXPHOS for ATP production enables activated microglia to produce ATP at a faster rate (Schuster, Boley, Moller, Stark, & Kaleta, 2015). Enhanced glycolysis supplies biosynthetic intermediates for cell growth and rapid production intermediates for cytokine production such as reactive oxygen species (ROS) thereby enabling effector functions (Chang et al., 2013; Everts et al., 2014). In macrophages or dendritic cells, pro-inflammatory stimuli cause them to undergo a metabolic switch from OXPHOS to glycolysis, a phenomenon similar to the Warburg effect (Kelly & O'Neill, 2015). Microglia share many functions and characteristics with macrophages (Butovsky & Weiner, 2018) but they are from a distinct non-hematopoietic lineage, and whether a similar switch from OXPHOS to glycolysis has not been explored in microglia.

We have previously found that both Toll-like receptor (TLR)-induced inflammation and mitochondrial dysfunction are involved in the development of neonatal brain injury

(Hagberg, Mallard, Rousset, & Thornton, 2014; Mottahedin et al., 2017). We have also found that mitochondrial ROS production and inflammation is increased after neonatal brain injury associated with altered Krebs cycle and succinate accumulation in the mitochondria (Koning et al., 2017). Activation of microglia results in an altered Krebs cycle, as a result of metabolic switch promoting inflammatory gene expression (Gimeno-Bayon, Lopez-Lopez, Rodriguez, & Mahy, 2014; Leaw et al., 2017; Orihuela et al., 2016). Katoh et al. found that that mitochondrial fission via the activation of DRP1 (by TLR4 stimulation) increases mitochondrial fission but they did not look in to metabolism or cytokine production in microglia (Katoh et al., 2017). Here, we add data on how TLR4 activation affects mitochondrial morphology, energy metabolism, ROS and cytokine production in microglia. This knowledge is important given the many roles of microglia in mediating host-defenses, and how these processes can mediate injury to the brain when activation is aberrant and prolonged. ROS signaling has been demonstrated to result in damage to cell components; at the same time ROS production is essential for host defenses (Y. Zhang et al., 2012).

In this study, we investigated the link between mitochondrial architecture and metabolic reprogramming in primary microglia after induction to a prototypical pro-inflammatory activation state via LPS-mediated TLR4 activation. We also used the putative mitochondrial fission inhibitor, Mdivi-1 (Cassidy-Stone et al., 2008) to modulate mitochondrial dynamics *in vitro* and *in vivo*. We found that pro-inflammatory activation of

microglia changes the mitochondrial dynamics including a metabolic switch from OXPHOS to glycolysis and that Mdivi-1 reverses these effects and the expected LPS-induced cytokine production and ROS production *in vitro*. Further, we investigated the effect of Mdivi-1 in an *in vivo* paradigm of neuroinflammation and found that Mdivi-1 reduced the expression of genes related to cytotoxic, repair and immunomodulatory microglia phenotypes.

Materials and Methods

Animals of *in vitro* experiments

Pregnant C57BL/6 mice were sourced from Charles River Laboratories International (Sulzfeld, Germany). C57BL/6J-Tg(CAG-Cox8/EGFP)49Rin mice (Cox8/EGFP; RBRC02250) expressing endogenous green florescent protein in cytochrome c oxidase, subunit VIIIa of mitochondria (Shitara et al., 2001) were obtained from Riken bio resource center, Japan. Animals were housed and bred at the Experimental Biomedicine animal facility (University of Gothenburg, Gothenburg, Sweden) under specific pathogen free conditions on a 12 h light/dark 7 cycle with *ad libitum* access to standard laboratory chow (B&K, Solna, Sweden) and water. All experiments were approved by the local ethical committee at University of Gothenburg (No: 203-2014 and 32-2016) and performed according to the Guidelines for the care and use of Laboratory Animals.

Microglial cell culture

Primary cultures of purified microglia were created from 1 to 3-day-old C57BL/6 or Cox8/EGFP mice of both sexes, as previously described (Dean et al., 2010) with minor adaptations. Following decapitation, the brain was isolated with the meninges removed and washed in ice-cold Hanks buffered salt solution (HBSS; Sigma–Aldrich, St Louis, MO, USA) supplemented with 100 U/mL penicillin and 100 µg/mL streptomycin (Sigma–Aldrich). Forebrains were dissociated by gentle trituration in Dulbecco's modified Eagle's medium (DMEM; Sigma–Aldrich) supplemented with 20% heat-inactivated fetal bovine serum (FBS; Fischer Scientific, Goteborg, Sweden) and antibiotics. The cell suspension was passed through a 70 µm cell sieve (Falcon, Corning, USA), plated in 75-cm^2 flasks with vented caps (Sarstedt, Germany) at a density of two brains/flask, and cultured undisturbed for seven days with HBSS/20% FBS/antibiotics. Medium was then replaced with HBSS/10% FBS/antibiotics, and cells were cultured for a further seven days. Microglia were selectively detached from the flasks by shaking (3 h, 37^0C, 250 rpm) on a rotary shaker and the microglia cell suspension was collected and centrifuged (250 g × 10 min). The media were then removed, the pellet was suspended in DMEM/2% FBS/antibiotics and the number of cells were counted with an automated cell counter (Scepter; Millipore) and seeded into Seahorse XFe96 or 24 cell well plates (1× 10^5 cells per well). The purity of microglia cells was evaluated by immunocytochemical staining using antibodies against ionized calcium binding adapter molecule 1 (Iba1; 1:1000; Wako Pure Chemical Industries, Ltd., Richmond, VA, USA) and DAPI (1:1000; Sigma–Aldrich),

and was routinely greater than 99%. All incubations were performed at 37° C in a humidified atmosphere containing 5% CO_2 and 95% air.

Sample Preparation for microscopy

Primary microglia cells cultured from Cox8/EGFP mice were used for mitochondrial morphology analysis. Microglia cells were washed with PBS and plated on precision cover glasses thickness No. 1.5H (tol. ± 5 µm) in a 24-well plate, with $1x10^5$ cells per well, and left to adhere overnight at 37°C in a cell culture incubator. Cells were fixed with 4% paraformaldehyde in culture media for 10 min and then mounted in ProLong Diamond antifade reagent (Life Technologies, Grand Island, NY) according to the manufacturer's instructions.

Live cell imaging

Primary microglia cells were seeded on MatTek (MatTek , Ashland, MA) glass bottom culture dishes. Following cell adherence, cells were exposed to DMSO alone (control) or LPS 100ng/ml for 24h or cells were pre-treated with Mdivi-1 (25 µM; Sigma, St. Louis, MO, USA) for 1h followed by LPS (100ng/ml) exposure for 24hrs. Cells were washed gently three times with warm PBS. Further anti-bleaching live cell visualization medium (DMEMgfp-2, Evrogen) was added to the cells 30 min before imaging. Images were acquired with a Zeiss LSM 880 Airyscan super-resolution system with live cell capabilities and fitted with a fast-ASmodule (Carl Zeiss, Oberkochen, Germany). Microscopes were

equipped with an environmental chamber that maintained 37^0C with humidified 5% CO_2 gas during imaging.

Super-Resolution Structured illumination microscopy (SR-SIM)

Super-resolution structured illumination microscopy (SR-SIM) on a Zeiss ELYRA PS.1 microscope (Carl Zeiss Microscopy, Germany) was used to yield a 2-fold improvement in all spatial directions (Huang, Bates, & Zhuang, 2009) beyond the classical Abbe-Rayleigh limit. GFP was imaged using a Plan-Apochromat 100×/1.4 oil objective, an excitation wavelength of 488 nm and an emission wavelength range of 495-575 nm. The SR-SIM images were acquired as z-stacks with three angles and five phases in each plane and the z-step between planes was 3.30 nm. SR-SIM processing was performed using the Zeiss Zen software package. 3D rendering was done using Volocity 6 (Perkin-Elmer) and figures were compiled using Photoshop CC software (Adobe Systems, San Jose, CA).

Mitochondrial morphology analysis

Primary microglia were treated with LPS, Mdivi-1 or DMSO as described previously and mitochondria were categorised based on length: fragmented (<1 μm), tubular (1–3 μm) and elongated (>3 μm), as described previously (Jahani-Asl et al., 2011). Over 20 cells were analysed in Control, LPS-treated, LPS plus Mdivi-1 in three independent experiments. Volocity 6 was used for 3D rendering and to quantify mitochondrial length, volume and number.

Measurement of Oxygen Consumption Rate (OCR) and Extracellular Acidification Rate (ECAR)

Real-time measurements of oxygen consumption rates, and extracellular acidification rates, a measure of lactate production, were performed on an XFe96 Seahorse extracellular flux analyser (Seahorse Biosciences, North Billerica, MA). The optimal seeding density and test compound concentrations were empirically determined prior to initiation of experiments. According to the methods described in the XFe96 Extracellular Flux Analyzer User Manual (Seahorse Bioscience), preliminary studies were run with Carbonyl cyanide-4-(trifluoromethoxy)phenylhydrazone (FCCP) to identify the optimal number of cells required to observe a sufficient shift in OCR and ECAR. Once the cell number was decided, we determined the optimal working concentrations for each of the stimulating compounds used in the mitochondrial function analysis (oligomycin, FCCP, and rotenone). Cells were then plated into XFe96 cell culture plates (Seahorse Biosciences, North Billerica, MA) at a density of 10,000/well in 80 µl of DMEM (Sigma–Aldrich, St Louis, MO, USA). Cells were allowed to adhere overnight in a 37°C incubator with 5% CO_2. Following cell adherence, cells were exposed to a final concentration of Ultra-pure LPS 50 or 100ng/ml (Escherichia coli 055: B5, Biological Laboratories, Campbell, CA) or media alone (control) for 3, 6 or 24 h. For mitochondrial fission blocking experiments, microglia cells were pre-treated with Mdivi-1 (25 µM) or DMSO for 1 h before LPS exposure. Media (80 µL) was removed followed by the addition of 200 µL XF base media (180 µl) supplemented with 10mM glucose, 5mM pyruvate, and 2mM glutamine for

OCR. For ECAR only 2mM glutamine was added following incubation in a non-CO_2 chamber for 1 h.

The day prior to the experiment, 200µl of XF calibration media was added to the XF sensor cartridges and kept in a non-CO_2 incubator for 24h. XF sensor cartridges were loaded with test compounds and OCR/ECAR measured. OCR was measured by sequential injections of oligomycin (1µM final concentration, blocks ATP synthase to assess respiration required for ATP turnover), FCCP (carbonyl cyanide 4-trifluoromethoxy-phenylhydrazone, 2µM final concentration, a proton ionophore uncoupler inducing maximal respiration), and rotenone plus antimycin A (1µM final concentration of each, which completely inhibits electron transport to measure non-mitochondrial respiration).

ECAR was measured under glucose-starved microglia. Basal glycolysis rate was determined by injecting glucose at a final concentration of 10mM. For estimating glycolytic capacity, oligomycin was injected at a final concentration of 5µM. Finally, 2-deoxyglucose (2-DG) was injected at a final concentration of 50mM to measure the non-glycolytic acidification. Each step had three cycles; each cycle consisted of 3 min mixing, 2 min incubation and 3 min measurement. All experiments were run in three replicates with 3-4 sample per replicates. Cell counts were used to normalize OCR and ECAR.

Multiplex cytokine assay

Bio-Plex Pro Mouse Cytokine Standard 23-Plex kit (Bio-Rad) was used to measure the concentrations of cytokines/chemokines in microglia-cultured media following the manufacturer's protocol. Microglia conditioned media was collected from microglia samples used in the OCR and ECAR experiments explained above. Samples were normalized to cell number ($1x10^5$; 1:10 in diluent buffer) and concentrations of IL-1α, IL-1β, IL-2, IL-3, IL-4, IL-5, IL-6, IL-9, IL-10, IL-12 (p40), IL-12 (p70), IL-13, IL-17a, eotaxin, granulocyte colony-stimulating factor (G-CSF), granulocyte macrophage colony-stimulating factor (GM-CSF), interferon-gamma (IFN-γ), KC/chemokine (C-X-C motif) ligand 1 (CXCL1), monocyte chemotactic protein-1 (MCP-1)/chemokine (C-C motif) ligand 2 (CCL2), macrophage inflammatory protein 1α (MIP-1α)/CCL3, MIP-1β/CCL4, RANTES, and TNF-α were simultaneously quantified on a Bio Plex 200 System (Bio-Rad, Sweden) and data presented as Log10 of cytokine concentrations (picograms per millilitre).

Succinate level measurement

Microglia cells were pre-treated with vehicle (DMSO), Mdivi-1 (25 μM; Sigma, St. Louis, MO, USA) for 1h or dimethyl malonate (DMM; 10mM; Sigma, St. Louis, MO, USA) for 3h before stimulation with LPS (100 ng/ml) for 24 h. Succinate Colorimetric Assay Kit (Sigma-Aldrich Inc., St Louis, MO, USA) was used to determine the succinate concentrations according to the manufacturer's instructions. Microglia cells (1×10^5 cells

per well) were rapidly homogenized on ice in 100µL of ice-cold succinate assay buffer and centrifuged at 10,000×g for 5 min to remove insoluble material. Then, cell homogenates were added into a 96-well plate in duplicate wells and mixed with reaction mix provided in with the kit, which results in a colorimetric product proportional to the succinate present. The resultant mixtures were further incubated at 37°C for 20 min. The succinate concentration was determined by the standard curve using spectroscopy at 450nm wavelength.

Measurement of mitochondrial ROS production by live cell imaging.

Mitochondrial superoxide generation was assessed in live cells using MitoSOX (Molecular Probes), a fluorogenic dye that is taken up by mitochondria, where it is readily oxidized by superoxide ($O2^{-\cdot}$). MitoSOX Red reagent is a novel fluorogenic dye specifically targeted to mitochondria in live cells. Oxidation of MitoSOX Red reagent produces red fluorescence by superoxide but not by other ROS or Reactive Nitrogen Species-generating systems. Primary microglia cells were seeded on MatTek (MatTek , Ashland, MA) glass bottom culture dishes ($1x10^5$cells/dish) and left to adhere overnight. Following treatments described above, live microglia were incubated with 5µM MitoSOX at 37^{o}C for 10 min. Cells were washed gently three times with warm PBS further anti-bleaching live cell visualization medium (DMEMgfp^{-2}) was added to the cells 30 min before imaging. Airyscan super-resolution microscopy on a LSM 880 (Carl Zeiss Microscopy, Germany) with an onboard incubator at 37^{o}C was used to acquire images using a 63× oil objective,

an excitation wavelength of 488nm. Airyscan-processing was done using the Zeiss Zen software package. MitoSox fluorescence was quantified using Volocity 6.

Measurement of the mitochondrial membrane potential by live cell imaging.

JC-1 (Molecular Probes) is a cationic dye that exhibits mitochondrial membrane potential-dependent accumulation in mitochondria, indicated by a fluorescence emission shift from green (~525 nm) to red (~590 nm). Mitochondrial depolarization is indicated by a decrease in the red to green fluorescence intensity ratio. The potential sensitive color shift is due to concentration dependent formation of red fluorescent aggregates. Primary microglia cells were seeded, incubated and treated as above. Following LPS exposure, the media was removed cells were incubated with JC-1 (2μM final concentration) and incubated at 37°C, 5% CO2 for 20 min. Cells were washed gently three times with warm PBS and further anti-bleaching live cell visualization medium (DMEMgfp^{-2}) was added to the cells 30 min before imaging. Images were scanned using an oil immersion, 63×, and 1.3 NA objective. Samples were excited at wavelength of 488nm and emission wavelength of 547 and 617 nm. The confocal pinhole aperture was set to 50, and the voltage to the photomultiplier tubes of each channel was maintained at equal values. Illumination was limited to periods of image acquisition. Images were exactly in phase and represented the amount of monomeric and J-aggregate JC-1 fluorescence.

Effect of Midivi-1 in an *in vivo* model of inflammation-mediated damage to the preterm brain

We employed a well characterized paradigm of systemic inflammation driven neuroinflammation (Favrais et al., 2011; Krishnan et al., 2017; Van Steenwinckel et al., 2018), which is known to have effects on brain development and behavior consistent with those reported in infants and children born preterm(Ball et al., 2017; Raju, Buist, Blaisdell, Moxey-Mims, & Saigal, 2017) . Experimental protocols were approved by the institutional guidelines of the Institute National de la Santé et de la Recherche Scientifique (Inserm) France. The treatments was carried out as per previously described in full(Favrais et al., 2011), with a shortened protocol described below. Assessment of gene expression were made only in male animals as female animals are not injured in this paradigm, mimicking the male predisposition to injury observed in male preterm born infants(Peacock, Marston, Marlow, Calvert, & Greenough, 2012). Briefly, mice received twice a day from P1 to P2 and once on P3 a 5-µl intra-peritoneal injection of 10 µg/kg/injection recombinant mouse IL-1β in phosphate buffered saline (PBS; R&D Systems, Minneapolis, MN) or PBS alone or P1–P3 pups were co-injected with IL-1β and 3 mg/kg/injection of Mdivi-1 (IP, 5ul).

Isolation and ex vivo microglia and gene expression analysis

At P3, brains were collected for cell dissociation and CD11B+ cell separation using a magnetic coupled antibody anti-CD11B (Miltenyi, MACS Technology) as previously

described in detail (Krishnan et al., 2017; Schang et al., 2014; Shiow et al., 2017). Microglia are the predominant CD11B cell in this model of injury by more than 100 fold compared to populations of either macrophage or neurtrophil (Krishnan et al., 2017). Total RNA was extracted from the CD11B+ microglia cells with the RNeasy mini kit (Qiagen, France), RNA quality and concentration were assessed by spectrophotometry (NanodropTM, Thermofisher Scientific, MA, USA). Reverse transcription was achieve with the iScriptTM cDNA synthesis kit (Bio-Rad, France) and RT-qPCR was performed in triplicate for each sample using SYBR Green Super- mix (Bio-Rad) as previously described (Chhor et al., 2013). Primers were designed using Primer3 plus software (See sequences in Sup. Table 1). Specific mRNA levels were calculated after normalization to Rpl13a mRNA (reference gene) based on previous reference gene suitability testing. The data are presented as relative mRNA units with respect to the control group (expressed as fold over control value).

Statistics

All statistics are reported as mean ± SEM, performed using GraphPad Prism 7.0 (GraphPad Software). Significance scores are * for $p < 0.05$, ** for $p < 0.01$, *** for $p < 0.001$ and **** $p<0.0001$.

Results

LPS exposure induces excessive mitochondrial fragmentation in microglial cells.

Mitochondrial morphology was examined in primary microglia cells cultured from Cox8-EGFP mice exposed to 50 or 100ng/mL LPS using 3D SR-SIM microscopy. The number of fragmented mitochondria was significantly increased in microglia cells stimulated with 100ng/ml LPS for 24h (Fig 1c), and elongated and tubular mitochondria were decreased compared with untreated controls (Fig 1g). These findings are in line with previous studies in BV2 cells (Park et al., 2013) and primary microglia but with a higher dose of LPS (1ug/ml) (Katoh et al., 2017). There was no change in the morphology of cells stimulated with 50ng/ml LPS for 24h (Fig 1b,g).

LPS induces a switch from oxidative phosphorylation (OXPHOS) to glycolysis (metabolic reprogramming) in microglia cells.

Oxygen consumption rates (OCR) and extracellular acidification rates (ECAR) was measured in real time as measures of mitochondrial respiration and glycolysis for 50ng/ml LPS (fig 2a-c & i-k) and 100ng/LPS (Fig. 2o-q & w-y) respectively (Wu et al., 2007) with the Seahorse XFe96. Basal OCR and ATP-linked OCR was significantly increased in microglia cells following exposure to 50ng/ml LPS for 6-24h compared to controls (Fig.2d-e). FCCP-induced maximal OCR and spare respiratory capacity (SRC) decreased whereas leak-driven OCR significantly increased with exposure to 50ng/mL of LPS (Fig. 2f-h). The ECAR parameters (glycolysis, glycolytic capacity and glycolytic reserve) were

359 increased following exposure to 50ng/ml LPS for 6-24hrs compared to controls (Fig. 2l-
360 n). These results show that a moderate dose of LPS increases both OCR and glycolysis.

361 Exposure to 100ng/mL of LPS for 6h resulted in an increase in basal OCR, ATP-linked
362 OCR and leak-linked OCR compared to controls (Fig. 2r-s). In contrast, there was a
363 significant decrease in basal OCR and ATP linked OCR at 24h after 100ng/mL LPS (Fig.
364 2r,s,u). FCCP-induced maximal OCR and SRC significantly decreased at 24h 100ng/mL
365 LPS (Fig. 2t-u). Glycolytic parameters increased with 100ng/ml LPS exposure for 3-24h
366 compared with controls (Fig.2w-y). The overall decrease in OCR and increase in ECAR
367 parameters with 100ng/ml LPS for 24h indicates a metabolic switch from OXPHOS to
368 glycolysis.

369 **Mdivi-1 treatment blocks LPS-induced mitochondrial fragmentation and ROS production.**
370 Many conserved GTPase proteins are involved in mitochondrial fusion and fission
371 dynamics such as mitofusins (MFN1 and MFN2) and dominant optic atrophy 1 (OPA1)
372 are needed for the fusion of mitochondrial outer and inner membranes (Song, Ghochani,
373 McCaffery, Frey, & Chan, 2009). Dynamin-related protein 1 (DRP1) and mitochondrial
374 Fission 1 protein (FIS1) are the main mitochondrial fission mediators (Frezza et al., 2006).
375 We used the mitochondrial fission inhibitor Mdivi-1 (Ruiz, Alberdi, & Matute, 2018) as the
376 high (100 ng/ml) dose of LPS induced an increase in fragmented mitochondria (Fig. 3b).
377 We examined the effect of pharmacologically blocking mitochondrial fission in LPS-
378 exposed microglia cells cultured from Cox8/EGFP mice by pre-treatment with 25 μM

Mdivi-1 for 1 h followed by incubation with LPS (100 ng/ml) for 24h. Results revealed that LPS-induced excessive mitochondrial fragmentation was significantly inhibited by Mdivi-1 pre-treatment and normalized mitochondrial morphology (Fig. 3c). Mdivi-1 treatment before LPS exposure reduced the number of fragmented mitochondria and increased the number of tubular and elongated mitochondria to control levels (Fig. 3d) .

Mdivi-1 treatment normalized oxygen consumption and extracellular acidification rate in the microglia cells.

Since Mdivi-1 restored mitochondrial morphology, we interrogated its effect on cellular respiration and ECAR-dependent glycolysis and glycolytic capacity (Fig. 4a, b, h, i). Mdivi-1 pre-treatment in cells exposed to LPS (100ng/ml for 6h) exhibited a decrease in the level of basal respiration and ATP-linked OCR to control levels compared to LPS treated cells (Fig. 4c-d). Conversely, Mdivi-1 treatment in cells exposed to 100ng LPS for 24h led to an increase in basal and ATP-linked OCR compared to non-treated LPS exposed cells (Fig. 4c-d). Mdivi-1 treatment also increased FCCP-induced maximal OCR at 24h and leak-driven OCR compared to LPS exposed cells at both time points (Fig. 4e-f). Administration of Mdivi-1 in combination with LPS normalized the spare respiratory capacity (Fig. 4g). ECAR measurements showed that glycolysis and glycolytic capacity was significantly reduced to control levels in Mdivi-1 treated cells at 6 and 24h 100ng/ml LPS exposure (Fig.4h-k) compared to LPS exposed cells.

Mdivi-1 reduces the LPS induced release of cytokines and chemokines.

To show how LPS activation was inducing an inflammatory reaction in the primary microglia and to test whether this was effected by Mdivi-1 we measured cytokine and chemokine response in microglia conditioned media after treatment with of LPS and or Mdivi-1 (supporting information Fig. S1 and S2). As expected both doses, of LPS led to a significant up-regulation of essentially all cytokines and chemokines compared to controls. In general there was much higher cytokine production in microglia exposed to 100ng-24h LPS conditioned media compared to 50ng-24hr LPS. We next determined if blockage of mitochondrial fission also modulated LPS-induced expression of cytokine and chemokine mediators. Mdivi-1 significantly reduced the pro-inflammatory cytokines (IL-1α, IL-6, TNF-α, IL-12(p40)), chemokines (G-CSF, CCL5, RANTES) and anti-inflammatory cytokines (IL-10, IL-13) and the chemokines (monocyte chemotactic protein 1 (MCP-1 β), in response to 100ng/ml of LPS for 24h. The LPS-induced production of IL-2, IL-5 and MIP1 α were not significantly reduced by Mdivi-1 (Fig.5).

Mdivi-1 suppresses LPS induced succinate production.

Succinate is a well-established pro-inflammatory metabolite that is known to accumulate during LPS induced macrophage activation (Mills et al., 2016) but the role of succinate during microglia activation needs further investigation. We found that LPS (100ng/ml) resulted in a significant increase of succinate (Fig.6a) accompanying the expression of pro/anti-inflammatory cytokines and chemokines. Mdivi-1 pretreatment (Fig 6a) or

418 blocking succinate production by succinate dehydrogenase inhibitor (DMM,10mM) (Fig.
419 6b) normalized succinate production. These results were further strengthened by the fact
420 that treatment with DMM or scavenging ROS production with NAC (10mM, 30 min)
421 recapitulated the effects of Mdivi-1 (Fig.5) by reducing pro/anti-inflammatory cytokines
422 and chemokine release (Supplementary figure S3). Excessive fission results in
423 fragmented mitochondria and causes a metabolic shift in microglia (Khacho et al., 2014)
424 from OCR to ECAR. This may result in increased succinate production which in turn acts
425 as a feedback loop to amplify aberrant mitochondrial fission (Lu et al., 2018).

426 **Inhibition of mitochondria fission by Mdivi-1 suppresses mitochondrial ROS production.**
427 Mitochondrial ROS plays an important role in LPS-induced immune responses (Park et
428 al., 2015). In order to examine the role of ROS production after LPS stimulation,
429 mitochondrial ROS (mtROS) was measured with MitoSOX, a mitochondrial superoxide
430 indicator. The fluorescence intensity of MitoSOX increased 24h after the LPS stimulation
431 (100ng/ml, 24h) (Fig. 7). Treatment with Mdivi-1 (25 μM, 1h) before LPS exposure
432 abolished the increase in MitoSOX fluorescence intensity observed 2h after the LPS
433 stimulation. These results indirectly show that that mitochondrial fission (induced by TLR4
434 stimulation) increases ROS production as shown in this study and others (Katoh et al.,
435 2017; Park et al., 2013).

436 **Mdivi-1 treatment attenuated LPS induced increase of mitochondrial membrane**
437 **potential**

438 Our data suggest that after LPS (100ng/ml) exposure for 24h microglia mainly depended
439 on glycolysis for energy production. Therefore, we investigated the mitochondrial
440 membrane potential using the mitochondrial membrane potential probe JC-1 in these
441 conditions. We found that there was a consequent elevation of mitochondrial membrane
442 potential and treatment with Mdivi-1 significantly reduced mitochondrial membrane
443 potential (525/565 nm) ratio compared to LPS treated group (Fig. 8).

444 **Mdivi-1 treatment attenuated microglial activation in a mouse paradigm of**
445 **neuroinflammation.**

446 Based on our working hypothesis that Mdivi-1 can reduce the inflammatory reaction of
447 microglia, we sought to investigate the potential for Mdivi-1 to reduce the activation of
448 microglia *in vivo* (Favrais et al., 2011; Krishnan et al., 2017). We isolated microglia from
449 the brains of animals at P3 following induction of systemically driven neuroinflammation
450 and con-current treatment with Mdivi-1 from P1-P3. We analyzed the isolated microglia
451 for gene expression of markers associated with functional phenotypes including cytotoxic
452 (*Nos2*, *Ptgs2*, *Cd32*), repair and regeneration (*Arg1*, *Lga3*, *Igf1*), and immunomodulatory
453 (*Il1ra*, *Il4a*, *Socs3*) phenotypes. Exposure to neuroinflammatory-stimuli affected the gene
454 expression as expected (Krishnan et al., 2017), with increased expression of all of the
455 genes except for the gene for IGF1, which was decreased. IGF1 is a pleotropic growth

456 factor necessary for myelonogenesis and known to be decreased by pro-inflammatory
457 microglial activation (Wlodarczyk et al., 2017). Mdivi-1 treatment normalized to control
458 (PBS) levels the expression of genes associated with cytotoxicity and
459 immunomodulation, but had no effect on IGF1 gene expression, and only partly recovered
460 Galectin-3 gene expression (*Lgal3*), indicating that exposure to Mdivi-1, which inhibits
461 mitochondrial fragmentation, modulates the microglial inflammatory response also *in* vivo
462 (Fig. 9).

463 ## Discussion

464 This study strengthens our knowledge of the links between mitochondrial architecture,
465 inflammation and energy metabolism in microglial cells. We have shown that activation
466 of microglia to a pro-inflammatory activation state increased mitochondrial fragmentation,
467 which was accompanied by a reduction in oxidative phosphorylation and an increase in
468 glycolysis, which was dose and time dependent. Pre-treatment with the putative
469 mitochondrial division inhibitor, Mdivi-1, normalised LPS-induced mitochondrial
470 fragmentation, normalised the cellular respiration and glycolysis to control levels. Mdivi-1
471 greatly reduced LPS-induced cytokine production normalized LPS-induced ROS
472 production and mitochondrial membrane potential.

473 Neuroinflammation includes complex changes in microglial phenotypes, mediated by
474 gene expression changes leading to the production of cytokines and chemokines and
475 production of ROS. Altogether this triggers oxidative and nitrosative stress in the brain

476 (Bolouri et al., 2014; Hellström Erkenstam et al., 2016). We observed as expected that
477 LPS-activated microglia produced a plethora of chemokines and cytokines and ROS. In
478 this pro-inflammatory scenario, suppression of LPS-induced mitochondrial ROS plays a
479 role in modulating the production of pro-inflammatory mediators by preventing MAPK and
480 NF-κB activation suggesting a potential therapy for inflammation-associated degenerative
481 neurological diseases (Park et al., 2015).

482 To understand LPS-induced changes in mitochondrial structure, we used high resolution
483 3D ELYRA-SIM (Shim et al., 2012) to quantify mitochondrial morphology which revealed
484 that high dose LPS for 24h increased fragmentation. A low dose of LPS caused an initial
485 increase in OCR which was not accompanied by any change in mitochondrial
486 morphology. However, a higher dose of LPS induced a decrease of OCR and a further
487 increase of ECAR which triggered mitochondrial fission. Fragmented mitochondria
488 constitute the preferred morphological state when respiratory activity is low (Westermann,
489 2012). A high or moderate dose of LPS caused a decrease in respiration and cells
490 became dependent on glycolysis favoring excessive fragmentation. The molecular
491 mechanisms behind this response is not known but it has been proposed that the energy
492 depletion elicits mitochondrial fragmentation and subsequent mitophagy (Youle & van der
493 Bliek, 2012). Increased mitochondrial fragmentation due to excessive fission can
494 exacerbate the inflammatory response of microglia (Ho et al., 2018) through modulation
495 of DRP1 de-phosphorylation and elimination of ROS (Park et al., 2016). We chose to use

Mdivi-1 a mitochondrial division inhibitor to study microglial metabolism as it related to mitochondrial morphology as previous studies revealed that LPS exposure in microglia cells leads to activation of mitochondrial fission protein DRP1 (Katoh et al., 2017; Park et al., 2013).

Mdivi-1 is a widely accepted DRP-1 mediated mitochondrial fission inhibitor used in many studies (Baek et al., 2017; Peiris-Pagès, Bonuccelli, Sotgia, & Lisanti, 2018; So, Hsing, Liang, & Wu, 2012; Xie et al., 2013) . Our data supports the assertion that changes in mitochondrial dynamics may be needed for the expression of inflammatory mediators in activated microglia cells. Mdivi-1 has previously been shown to attenuate LPS-induced ROS and proinflammatory mediator production in a BV-2 microglial cell line (Park et al., 2013) with a very high dose of 1ug/ml. BV2 cells are similar to primary microglia (Henn et al., 2009), but they contain oncogenes that render them phenotypically different with regard to e.g. proliferation and adhesion (Horvath, Nutile-McMenemy, Alkaitis, & Deleo, 2008). Our findings not only show that pre-treatment with Mdivi-1 reduced LPS-induced mitochondrial fragmentation and expression of pro-inflammatory mediators, but also normalized mitochondrial function in microglia. These data support the suggestion that increasing the fusion/fission ratio reduces the extent of neuroinflammation (Kim, Lee, Park, Kim, & Roh, 2016). To further support the potential validity of targeting fission as a therapeutic strategy, we tested the ability of Mdivi-1 to modify microglial activity *in vivo*. We used a paradigm of systemically driven neuroinflammation, wherein an IP injection of

516 the inflammatory agent interleukin-1β induces a highly complex neuroinflammatory
517 reaction involving microglia (Krishnan et al., 2017; Van Steenwinckel et al., 2018).
518 Supporting our in vitro data mdivi-1 was able to reduce the expression of genes
519 associated with classically pro-inflammatory genes, and the anti-inflammatory activation
520 state, which is associated with the *in vivo* inflammatory reaction.

521 Previous work with BV2 demonstrated that LPS causes an inhibition of OXPHOS
522 (Voloboueva, Emery, Sun, & Giffard, 2013). However, this study used a very high dose
523 of LPS (1μg/ml) which is shown to elicit mitochondrial toxicity (Ahn et al., 2012). We
524 demonstrate for the first time that a low or moderate dose of LPS (50ng/ml) results in an
525 increase of ATP linked OCR and basal respiration in support of another study in skeletal
526 muscle cells where they used a very low dose of LPS in isolated mitochondria (Frisard et
527 al., 2015). High dose of LPS (100ng/ml) caused a decrease in FCCP induced maximal
528 respiration and an increase in leak-driven respiration. A depletion of spare respiratory
529 capacity was found at 6 and 24h following LPS exposure. However, we have noted no
530 significant difference in cell viability or death after LPS.

531 OCR exhibited a biphasic response characterized initially by an increase of OCR in
532 response to low LPS and then a marked drop of OCR after moderate to high doses of
533 LPS whereas ECAR increased in proportion to the dose of LPS. We interpret the initial
534 increase of OCR as a means to match an increased demand of ATP. However, as the
535 pro-inflammatory stimulus becomes stronger it appears favourable to shift from

mitochondrial respiration to aerobic glycolysis (Warburg effect) in order to promote more rapid ATP production (Kelly & O'Neill, 2015; Orihuela et al., 2016) and synthesis of inflammatory mediators such as cytokines/chemokines and ROS (Kelly & O'Neill, 2015). We believe the Warburg effect is an important concept for understanding metabolic changes occurring during microglial activation. It is shown that also activation of macrophages or dendritic cells (DCs) with LPS, induces a metabolic switch from OXPHOS to glycolysis (Krawczyk et al., 2010). Metabolic shift may be facilitated by increased mitochondrial fission and/or reduced fusion mediated by DRP1 activation (Baker, Maitra, Geng, & Li, 2014). However, as glycolysis is less efficient at producing ATP than OXPHOS, this metabolic reorientation cannot solely be to meet energy demands. Glycolysis may also facilitate in cytokine production by producing intermediate metabolites (Mills et al., 2016). A previous study found that glycolysis was required to produce optimal IFN-γ during T cell activation and is translationally regulated by the binding of the glycolysis enzyme GAPDH to IFN-γ mRNA (Chang et al., 2013).

Our results in microglia add to what has already been shown in DCs and macrophages (Williams & O'Neill, 2018), specifically that pro-inflammatory activation resulted in increased succinate accumulation. In dendritic cells (DCs) and macrophages this succinate accumulation was related to an altered Krebs cycle and this was was normalized by Mdivi-1. Aberrant mitochondrial fission alters the Krebs cycle, by interfering with the processes after citrate and after succinate (Jha et al., 2015) by reducing of

556 cytochrome c oxidase and succinate dehydrogenase activity (B. Zhang et al., 2013).
557 Impaired succinate dehydrogenase activity results in succinate accumulation due to
558 impaired succinate to fumarate conversion (Mills et al., 2016). Accumulated succinate
559 drives reverse electron transport (RET) to generate excessive mitochondrial ROS
560 production (Chouchani et al., 2014; Niatsetskaya et al., 2012). Our data support this link
561 between accumulation of succinate and ROS production, which was prevented by Mdivi-
562 1.

563 LPS induced an increase in membrane potential and proton with an increase in
564 membrane potential. Proton leak is partly mediated by uncoupling proteins (UCPs)
565 present in the mitochondrial inner membrane (Hass & Barnstable, 2016; Krauss, Zhang,
566 & Lowell, 2005). It is shown that in primary microglia LPS induces an increase in UCP2
567 levels and membrane potential. UCP2-silenced microglia stimulated with LPS show a
568 decrease in membrane potential (De Simone et al., 2015). In macrophages LPS
569 stimulation repurpose their mitochondria from ATP production to succinate-dependent
570 ROS generation, with glycolysis taking on the role of ATP generation. In this case
571 mitochondria sustain a high membrane potential because protons generated by the
572 electron transport chain to make ATP are no longer being consumed by mitochondrial
573 ATP synthase (Mills et al., 2016). Macrophages can also reorganize their respiratory
574 chain in response to a bacterial infection, decreasing Complex I levels and increasing
575 the activity of Complex II (Garaude et al., 2016). These changes boost production of pro-

inflammatory cytokines such as interleukin 1β (IL-1β) and IL-10. Our data support these findings as normalizing mitochondrial membrane potential and ROS production with Mdivi-1 abolished pro- and anti-inflammatory cytokine and chemokine release.

Aberrant activation of microglial affects neurodegenerative processes through various neurotoxic cascades. We have shown that pro-inflammatory microglial activation alters cellular bioenergetics by inducing mitochondrial dysfunction and promoting a switch to glycolysis, supported by excessive mitochondrial fragmentation and increased cytokine output. This is likely an adaptive mechanism as the transition of sensing and surveying microglia into an activated state is likely to be accompanied by significantly increased energy consumption. Preventing excessive mitochondrial fission in microglial cells stimulated with LPS using a fission inhibitor Mdivi-1 normalizes mitochondrial respiration and glycolysis and attenuates the release of cytokines/chemokines. These lines of *in vitro* morphological and functional data and the *in vivo* data suggest that regulating mitochondrial dynamics may be a useful therapeutic modality for preventing neurological disorders caused by aberrant microglia activation.

References

Ahn, S. K., Hong, S., Park, Y. M., Choi, J. Y., Lee, W. T., Park, K. A., & Lee, J. E. (2012). Protective effects of agmatine on lipopolysaccharide-injured microglia and inducible nitric oxide synthase activity. *Life Sciences, 91*(25), 1345-1350. doi:https://doi.org/10.1016/j.lfs.2012.10.010

Baek, S. H., Park, S. J., Jeong, J. I., Kim, S. H., Han, J., Kyung, J. W., . . . Jo, D. G. (2017). Inhibition of Drp1 Ameliorates Synaptic Depression, Abeta Deposition,

and Cognitive Impairment in an Alzheimer's Disease Model. *J Neurosci, 37*(20), 5099-5110. doi:10.1523/jneurosci.2385-16.2017

Baker, B., Maitra, U., Geng, S., & Li, L. (2014). Molecular and Cellular Mechanisms Responsible for Cellular Stress and Low-grade Inflammation Induced by a Super-low Dose of Endotoxin. *J Biol Chem, 289*(23), 16262-16269. doi:10.1074/jbc.M114.569210

Ball, G., Aljabar, P., Nongena, P., Kennea, N., Gonzalez-Cinca, N., Falconer, S., . . . Edwards, A. D. (2017). Multimodal image analysis of clinical influences on preterm brain development. *Annals of Neurology*. doi:10.1002/ana.24995

Bolouri, H., Savman, K., Wang, W., Thomas, A., Maurer, N., Dullaghan, E., . . . Mallard, C. (2014). Innate defense regulator peptide 1018 protects against perinatal brain injury. *Ann Neurol, 75*(3), 395-410. doi:10.1002/ana.24087

Buck, M. D., O'Sullivan, D., Klein Geltink, R. I., Curtis, J. D., Chang, C. H., Sanin, D. E., . . . Pearce, E. L. (2016). Mitochondrial Dynamics Controls T Cell Fate through Metabolic Programming. *Cell, 166*(1), 63-76. doi:10.1016/j.cell.2016.05.035

Butovsky, O., & Weiner, H. L. (2018). Microglial signatures and their role in health and disease. *Nat Rev Neurosci*. doi:10.1038/s41583-018-0057-5

Cassidy-Stone, A., Chipuk, J. E., Ingerman, E., Song, C., Yoo, C., Kuwana, T., . . . Nunnari, J. (2008). Chemical inhibition of the mitochondrial division dynamin reveals its role in Bax/Bak-dependent mitochondrial outer membrane permeabilization. *Dev Cell, 14*(2), 193-204. doi:10.1016/j.devcel.2007.11.019

Chang, C. H., Curtis, J. D., Maggi, L. B., Jr., Faubert, B., Villarino, A. V., O'Sullivan, D., . . . Pearce, E. L. (2013). Posttranscriptional control of T cell effector function by aerobic glycolysis. *Cell, 153*(6), 1239-1251. doi:10.1016/j.cell.2013.05.016

Chhor, V., Le Charpentier, T., Lebon, S., Ore, M. V., Celador, I. L., Josserand, J., . . . Fleiss, B. (2013). Characterization of phenotype markers and neuronotoxic potential of polarised primary microglia in vitro. *Brain, Behavior, and Immunity, 32*, 70-85. doi:10.1016/j.bbi.2013.02.005

Chouchani, E. T., Pell, V. R., Gaude, E., Aksentijević, D., Sundier, S. Y., Robb, E. L., . . . Murphy, M. P. (2014). Ischaemic accumulation of succinate controls reperfusion

injury through mitochondrial ROS. *Nature, 515*(7527), 431-435. doi:10.1038/nature13909

De Simone, R., Ajmone-Cat, M. A., Pandolfi, M., Bernardo, A., De Nuccio, C., Minghetti, L., & Visentin, S. (2015). The mitochondrial uncoupling protein-2 is a master regulator of both M1 and M2 microglial responses. *J Neurochem, 135*(1), 147-156. doi:10.1111/jnc.13244

Dean, J. M., Wang, X., Kaindl, A. M., Gressens, P., Fleiss, B., Hagberg, H., & Mallard, C. (2010). Microglial MyD88 signaling regulates acute neuronal toxicity of LPS-stimulated microglia in vitro. *Brain Behav Immun, 24*(5), 776-783. doi:10.1016/j.bbi.2009.10.018

Everts, B., Amiel, E., Huang, S. C.-C., Smith, A. M., Chang, C.-H., Lam, W. Y., . . . Pearce, E. J. (2014). TLR-driven early glycolytic reprogramming via the kinases TBK1-IKKε supports the anabolic demands of dendritic cell activation. *Nat Immunol, 15*(4), 323-332. doi:10.1038/ni.2833

Favrais, G., van de Looij, Y., Fleiss, B., Ramanantsoa, N., Bonnin, P., Stoltenburg-Didinger, G., . . . Gressens, P. (2011). Systemic inflammation disrupts the developmental program of white matter. *Annals of Neurology, 70*(4), 550-565. doi:10.1002/ana.22489

Frezza, C., Cipolat, S., Martins de Brito, O., Micaroni, M., Beznoussenko, G. V., Rudka, T., . . . Scorrano, L. (2006). OPA1 controls apoptotic cristae remodeling independently from mitochondrial fusion. *Cell, 126*(1), 177-189. doi:10.1016/j.cell.2006.06.025

Frisard, M. I., Wu, Y., McMillan, R. P., Voelker, K. A., Wahlberg, K. A., Anderson, A. S., . . . Hulver, M. W. (2015). Low levels of lipopolysaccharide modulate mitochondrial oxygen consumption in skeletal muscle. *Metabolism: clinical and experimental, 64*(3), 416-427. doi:10.1016/j.metabol.2014.11.007

Garaude, J., Acin-Perez, R., Martinez-Cano, S., Enamorado, M., Ugolini, M., Nistal-Villan, E., . . . Sancho, D. (2016). Mitochondrial respiratory-chain adaptations in macrophages contribute to antibacterial host defense. *Nat Immunol, 17*(9), 1037-1045. doi:10.1038/ni.3509

Gimeno-Bayon, J., Lopez-Lopez, A., Rodriguez, M. J., & Mahy, N. (2014). Glucose pathways adaptation supports acquisition of activated microglia phenotype. *J Neurosci Res, 92*(6), 723-731. doi:10.1002/jnr.23356

Greter, M., Lelios, I., & Croxford, A. L. (2015). Microglia Versus Myeloid Cell Nomenclature during Brain Inflammation. *Frontiers in Immunology, 6*, 249. doi:10.3389/fimmu.2015.00249

Hackenbrock, C. R. (1966). Ultrastructural bases for metabolically linked mechanical activity in mitochondria. I. Reversible ultrastructural changes with change in metabolic steady state in isolated liver mitochondria. *J Cell Biol, 30*(2), 269-297.

Hagberg, H., Mallard, C., Rousset, C. I., & Thornton, C. (2014). Mitochondria: hub of injury responses in the developing brain. *Lancet Neurol, 13*(2), 217-232. doi:10.1016/s1474-4422(13)70261-8

Hass, D. T., & Barnstable, C. J. (2016). Uncoupling protein 2 in the glial response to stress: implications for neuroprotection. *Neural regeneration research, 11*(8), 1197-1200. doi:10.4103/1673-5374.189159

Hellström Erkenstam, N., Smith, P. L. P., Fleiss, B., Nair, S., Svedin, P., Wang, W., . . . Mallard, C. (2016). Temporal Characterization of Microglia/Macrophage Phenotypes in a Mouse Model of Neonatal Hypoxic-Ischemic Brain Injury. *Frontiers in Cellular Neuroscience, 10*, 286. doi:10.3389/fncel.2016.00286

Henn, A., Lund, S., Hedtjarn, M., Schrattenholz, A., Porzgen, P., & Leist, M. (2009). The suitability of BV2 cells as alternative model system for primary microglia cultures or for animal experiments examining brain inflammation. *ALTEX, 26*(2), 83-94.

Ho, D. H., Je, A. R., Lee, H., Son, I., Kweon, H. S., Kim, H. G., & Seol, W. (2018). LRRK2 Kinase Activity Induces Mitochondrial Fission in Microglia via Drp1 and Modulates Neuroinflammation. *Exp Neurobiol, 27*(3), 171-180. doi:10.5607/en.2018.27.3.171

Horvath, R. J., Nutile-McMenemy, N., Alkaitis, M. S., & Deleo, J. A. (2008). Differential migration, LPS-induced cytokine, chemokine, and NO expression in immortalized BV-2 and HAPI cell lines and primary microglial cultures. *J Neurochem, 107*(2), 557-569. doi:10.1111/j.1471-4159.2008.05633.x

Huang, B., Bates, M., & Zhuang, X. (2009). Super resolution fluorescence microscopy. *Annual review of biochemistry, 78*, 993-1016. doi:10.1146/annurev.biochem.77.061906.092014

Jahani-Asl, A., Pilon-Larose, K., Xu, W., MacLaurin, J. G., Park, D. S., McBride, H. M., & Slack, R. S. (2011). The mitochondrial inner membrane GTPase, optic atrophy 1 (Opa1), restores mitochondrial morphology and promotes neuronal survival following excitotoxicity. *J Biol Chem, 286*(6), 4772-4782. doi:10.1074/jbc.M110.167155

Jha, Abhishek K., Huang, Stanley C.-C., Sergushichev, A., Lampropoulou, V., Ivanova, Y., Loginicheva, E., . . . Artyomov, Maxim N. (2015). Network Integration of Parallel Metabolic and Transcriptional Data Reveals Metabolic Modules that Regulate Macrophage Polarization. *Immunity, 42*(3), 419-430. doi:https://doi.org/10.1016/j.immuni.2015.02.005

Katoh, M., Wu, B., Nguyen, H. B., Thai, T. Q., Yamasaki, R., Lu, H., . . . Ohno, N. (2017). Polymorphic regulation of mitochondrial fission and fusion modifies phenotypes of microglia in neuroinflammation. *Scientific Reports, 7*(1), 4942. doi:10.1038/s41598-017-05232-0

Kelly, B., & O'Neill, L. A. J. (2015). Metabolic reprogramming in macrophages and dendritic cells in innate immunity. *Cell Research, 25*(7), 771-784. doi:10.1038/cr.2015.68

Khacho, M., Tarabay, M., Patten, D., Khacho, P., MacLaurin, J. G., Guadagno, J., . . . Slack, R. S. (2014). Acidosis overrides oxygen deprivation to maintain mitochondrial function and cell survival. *Nat Commun, 5*, 3550. doi:10.1038/ncomms4550

Kim, H., Lee, J. Y., Park, K. J., Kim, W.-H., & Roh, G. S. (2016). A mitochondrial division inhibitor, Mdivi-1, inhibits mitochondrial fragmentation and attenuates kainic acid-induced hippocampal cell death. *BMC Neuroscience, 17*, 33. doi:10.1186/s12868-016-0270-y

Koning, G., Leverin, A. L., Nair, S., Schwendimann, L., Ek, J., Carlsson, Y., . . . Hagberg, H. (2017). Magnesium induces preconditioning of the neonatal brain

via profound mitochondrial protection. *J Cereb Blood Flow Metab*, 271678x17746132. doi:10.1177/0271678x17746132

Krauss, S., Zhang, C.-Y., & Lowell, B. B. (2005). The mitochondrial uncoupling-protein homologues. *Nature Reviews Molecular Cell Biology, 6*, 248. doi:10.1038/nrm1592

Krawczyk, C. M., Holowka, T., Sun, J., Blagih, J., Amiel, E., DeBerardinis, R. J., . . . Pearce, E. J. (2010). Toll-like receptor-induced changes in glycolytic metabolism regulate dendritic cell activation. *Blood, 115*(23), 4742-4749. doi:10.1182/blood-2009-10-249540

Krishnan, M. L., Van Steenwinckel, J., Schang, A. L., Yan, J., Arnadottir, J., Le Charpentier, T., . . . Gressens, P. (2017). Integrative genomics of microglia implicates DLG4 (PSD95) in the white matter development of preterm infants. *Nat Commun, 8*(1), 428. doi:10.1038/s41467-017-00422-w

Leaw, B., Nair, S., Lim, R., Thornton, C., Mallard, C., & Hagberg, H. (2017). Mitochondria, Bioenergetics and Excitotoxicity: New Therapeutic Targets in Perinatal Brain Injury. *Frontiers in Cellular Neuroscience, 11*(199). doi:10.3389/fncel.2017.00199

Lu, Y.-T., Li, L.-Z., Yang, Y.-L., Yin, X., Liu, Q., Zhang, L., . . . Qi, L.-W. (2018). Succinate induces aberrant mitochondrial fission in cardiomyocytes through GPR91 signaling. *Cell Death & Disease, 9*(6), 672. doi:10.1038/s41419-018-0708-5

Mills, E. L., Kelly, B., Logan, A., Costa, A. S., Varma, M., Bryant, C. E., . . . O'Neill, L. A. (2016). Succinate Dehydrogenase Supports Metabolic Repurposing of Mitochondria to Drive Inflammatory Macrophages. *Cell, 167*(2), 457-470 e413. doi:10.1016/j.cell.2016.08.064

Moss, D. W., & Bates, T. E. (2001). Activation of murine microglial cell lines by lipopolysaccharide and interferon-gamma causes NO-mediated decreases in mitochondrial and cellular function. *Eur J Neurosci, 13*(3), 529-538.

Mottahedin, A., Svedin, P., Nair, S., Mohn, C. J., Wang, X., Hagberg, H., . . . Mallard, C. (2017). Systemic activation of Toll-like receptor 2 suppresses mitochondrial

748 respiration and exacerbates hypoxic-ischemic injury in the developing brain. *J*
749 *Cereb Blood Flow Metab*, 271678x17691292. doi:10.1177/0271678x17691292
750 Nasrallah, C. M., & Horvath, T. L. (2014). Mitochondrial dynamics in the central
751 regulation of metabolism. *Nat Rev Endocrinol, 10*(11), 650-658.
752 doi:10.1038/nrendo.2014.160
753 Niatsetskaya, Z. V., Sosunov, S. A., Matsiukevich, D., Utkina-Sosunova, I. V., Ratner,
754 V. I., Starkov, A. A., & Ten, V. S. (2012). The oxygen free radicals originating
755 from mitochondrial complex I contribute to oxidative brain injury following
756 hypoxia-ischemia in neonatal mice. *J Neurosci, 32*(9), 3235-3244.
757 doi:10.1523/jneurosci.6303-11.2012
758 Orihuela, R., McPherson, C. A., & Harry, G. J. (2016). Microglial M1/M2 polarization and
759 metabolic states. *Br J Pharmacol, 173*(4), 649-665. doi:10.1111/bph.13139
760 Park, J., Choi, H., Kim, B., Chae, U., Lee, D. G., Lee, S. R., . . . Lee, D. S. (2016).
761 Peroxiredoxin 5 (Prx5) decreases LPS-induced microglial activation through
762 regulation of Ca(2+)/calcineurin-Drp1-dependent mitochondrial fission. *Free*
763 *Radic Biol Med, 99*, 392-404. doi:10.1016/j.freeradbiomed.2016.08.030
764 Park, J., Choi, H., Min, J. S., Park, S. J., Kim, J. H., Park, H. J., . . . Lee, D. S. (2013).
765 Mitochondrial dynamics modulate the expression of pro-inflammatory mediators
766 in microglial cells. *J Neurochem, 127*(2), 221-232. doi:10.1111/jnc.12361
767 Park, J., Min, J. S., Kim, B., Chae, U. B., Yun, J. W., Choi, M. S., . . . Lee, D. S. (2015).
768 Mitochondrial ROS govern the LPS-induced pro-inflammatory response in
769 microglia cells by regulating MAPK and NF-kappaB pathways. *Neurosci Lett,*
770 *584*, 191-196. doi:10.1016/j.neulet.2014.10.016
771 Peacock, J. L., Marston, L., Marlow, N., Calvert, S. A., & Greenough, A. (2012).
772 Neonatal and infant outcome in boys and girls born very prematurely. *Pediatric*
773 *Research, 71*(3), 305-310. doi:10.1038/pr.2011.50
774 Peiris-Pagès, M., Bonuccelli, G., Sotgia, F., & Lisanti, M. P. (2018). Mitochondrial fission
775 as a driver of stemness in tumor cells: mDIVI1 inhibits mitochondrial function, cell
776 migration and cancer stem cell (CSC) signalling. *Oncotarget, 9*(17), 13254-
777 13275. doi:10.18632/oncotarget.24285

778 Pickles, S., Vigie, P., & Youle, R. J. (2018). Mitophagy and Quality Control Mechanisms
779 in Mitochondrial Maintenance. *Curr Biol, 28*(4), R170-r185.
780 doi:10.1016/j.cub.2018.01.004
781 Raju, T. N. K., Buist, A. S., Blaisdell, C. J., Moxey-Mims, M., & Saigal, S. (2017). Adults
782 born preterm: a review of general health and system-specific outcomes. *Acta*
783 *Paediatrica*. doi:10.1111/apa.13880
784 Ruiz, A., Alberdi, E., & Matute, C. (2018). Mitochondrial Division Inhibitor 1 (mdivi-1)
785 Protects Neurons against Excitotoxicity through the Modulation of Mitochondrial
786 Function and Intracellular Ca(2+) Signaling. *Frontiers in Molecular Neuroscience,*
787 *11*, 3. doi:10.3389/fnmol.2018.00003
788 Schang, A.-L., Van Steenwinckel, J., Chevenne, D., Alkmark, M., Hagberg, H.,
789 Gressens, P., & Fleiss, B. (2014). Failure of thyroid hormone treatment to
790 prevent inflammation-induced white matter injury in the immature brain. *Brain*
791 *Behav Immun, 37*(100), 95-102. doi:10.1016/j.bbi.2013.11.005
792 Schuster, S., Boley, D., Moller, P., Stark, H., & Kaleta, C. (2015). Mathematical models
793 for explaining the Warburg effect: a review focussed on ATP and biomass
794 production. *Biochem Soc Trans, 43*(6), 1187-1194. doi:10.1042/bst20150153
795 Shim, S. H., Xia, C., Zhong, G., Babcock, H. P., Vaughan, J. C., Huang, B., . . . Zhuang,
796 X. (2012). Super-resolution fluorescence imaging of organelles in live cells with
797 photoswitchable membrane probes. *Proc Natl Acad Sci U S A, 109*(35), 13978-
798 13983. doi:10.1073/pnas.1201882109
799 Shiow, L. R., Favrais, G., Schirmer, L., Schang, A. L., Cipriani, S., Andres, C., . . .
800 Rowitch, D. H. (2017). Reactive astrocyte COX2-PGE2 production inhibits
801 oligodendrocyte maturation in neonatal white matter injury. *Glia, 65*(12), 2024-
802 2037. doi:10.1002/glia.23212
803 Shitara, H., Kaneda, H., Sato, A., Iwasaki, K., Hayashi, J., Taya, C., & Yonekawa, H.
804 (2001). Non-invasive visualization of sperm mitochondria behavior in transgenic
805 mice with introduced green fluorescent protein (GFP). *FEBS Lett, 500*(1-2), 7-11.
806 So, E. C., Hsing, C. H., Liang, C. H., & Wu, S. N. (2012). The actions of mdivi-1, an
807 inhibitor of mitochondrial fission, on rapidly activating delayed-rectifier K(+)

current and membrane potential in HL-1 murine atrial cardiomyocytes. *Eur J Pharmacol, 683*(1-3), 1-9. doi:10.1016/j.ejphar.2012.02.012

Solito, E., & Sastre, M. (2012). Microglia Function in Alzheimer's Disease. *Frontiers in Pharmacology, 3*, 14. doi:10.3389/fphar.2012.00014

Song, Z., Ghochani, M., McCaffery, J. M., Frey, T. G., & Chan, D. C. (2009). Mitofusins and OPA1 mediate sequential steps in mitochondrial membrane fusion. *Mol Biol Cell, 20*(15), 3525-3532. doi:10.1091/mbc.E09-03-0252

Tay, T. L., Savage, J. C., Hui, C. W., Bisht, K., & Tremblay, M. E. (2017). Microglia across the lifespan: from origin to function in brain development, plasticity and cognition. *J Physiol, 595*(6), 1929-1945. doi:10.1113/JP272134

Thion, M. S., Low, D., Silvin, A., Chen, J., Grisel, P., Schulte-Schrepping, J., . . . Garel, S. (2018). Microbiome Influences Prenatal and Adult Microglia in a Sex-Specific Manner. *Cell, 172*(3), 500-516.e516. doi:10.1016/j.cell.2017.11.042

Wai, T., & Langer, T. (2016). Mitochondrial Dynamics and Metabolic Regulation. *Trends in Endocrinology & Metabolism, 27*(2), 105-117. doi:https://doi.org/10.1016/j.tem.2015.12.001

Van Steenwinckel, J., Schang, A. L., Krishnan, M. L., Degos, V., Delahaye-Duriez, A., Bokobza, C., . . . Gressens, P. (2018). Loss of the Wnt/β-catenin pathway in microglia of the developing brain drives pro-inflammatory activation leading to white matter injury. *Biorxiv preprint*. doi:https://doi.org/10.1101/334359

Westermann, B. (2012). Bioenergetic role of mitochondrial fusion and fission. *Biochim Biophys Acta, 1817*(10), 1833-1838. doi:10.1016/j.bbabio.2012.02.033

Williams, N. C., & O'Neill, L. A. J. (2018). A Role for the Krebs Cycle Intermediate Citrate in Metabolic Reprogramming in Innate Immunity and Inflammation. *Frontiers in Immunology, 9*(141). doi:10.3389/fimmu.2018.00141

Wlodarczyk, A., Holtman, I. R., Krueger, M., Yogev, N., Bruttger, J., Khorooshi, R., . . . Owens, T. (2017). A novel microglial subset plays a key role in myelinogenesis in developing brain. *EMBO Journal*. doi:10.15252/embj.201696056

Voloboueva, L. A., Emery, J. F., Sun, X., & Giffard, R. G. (2013). Inflammatory response of microglial BV-2 cells includes a glycolytic shift and is modulated by

838 mitochondrial glucose-regulated protein 75/mortalin. *FEBS Lett, 587*(6), 756-762.
839 doi:10.1016/j.febslet.2013.01.067
840 Wu, M., Neilson, A., Swift, A. L., Moran, R., Tamagnine, J., Parslow, D., . . . Ferrick, D.
841 A. (2007). Multiparameter metabolic analysis reveals a close link between
842 attenuated mitochondrial bioenergetic function and enhanced glycolysis
843 dependency in human tumor cells. *Am J Physiol Cell Physiol, 292*(1), C125-136.
844 doi:10.1152/ajpcell.00247.2006
845 Xie, N., Wang, C., Lian, Y., Zhang, H., Wu, C., & Zhang, Q. (2013). A selective inhibitor
846 of Drp1, mdivi-1, protects against cell death of hippocampal neurons in
847 pilocarpine-induced seizures in rats. *Neurosci Lett, 545*, 64-68.
848 doi:10.1016/j.neulet.2013.04.026
849 Youle, R. J., & van der Bliek, A. M. (2012). Mitochondrial fission, fusion, and stress.
850 *Science (New York, N.Y.), 337*(6098), 1062-1065. doi:10.1126/science.1219855
851 Zhang, B., Davidson, M. M., Zhou, H., Wang, C., Walker, W. F., & Hei, T. K. (2013).
852 Cytoplasmic irradiation results in mitochondrial dysfunction and DRP1-dependent
853 mitochondrial fission. *Cancer Res, 73*(22), 6700-6710. doi:10.1158/0008-
854 5472.can-13-1411
855 Zhang, Y., Liao, S., Yang, M., Liang, X., Poon, M. W., Wong, C. Y., . . . Lian, Q. (2012).
856 Improved cell survival and paracrine capacity of human embryonic stem cell-
857 derived mesenchymal stem cells promote therapeutic potential for pulmonary
858 arterial hypertension. *Cell Transplant, 21*(10), 2225-2239.
859 doi:10.3727/096368912x653020

860

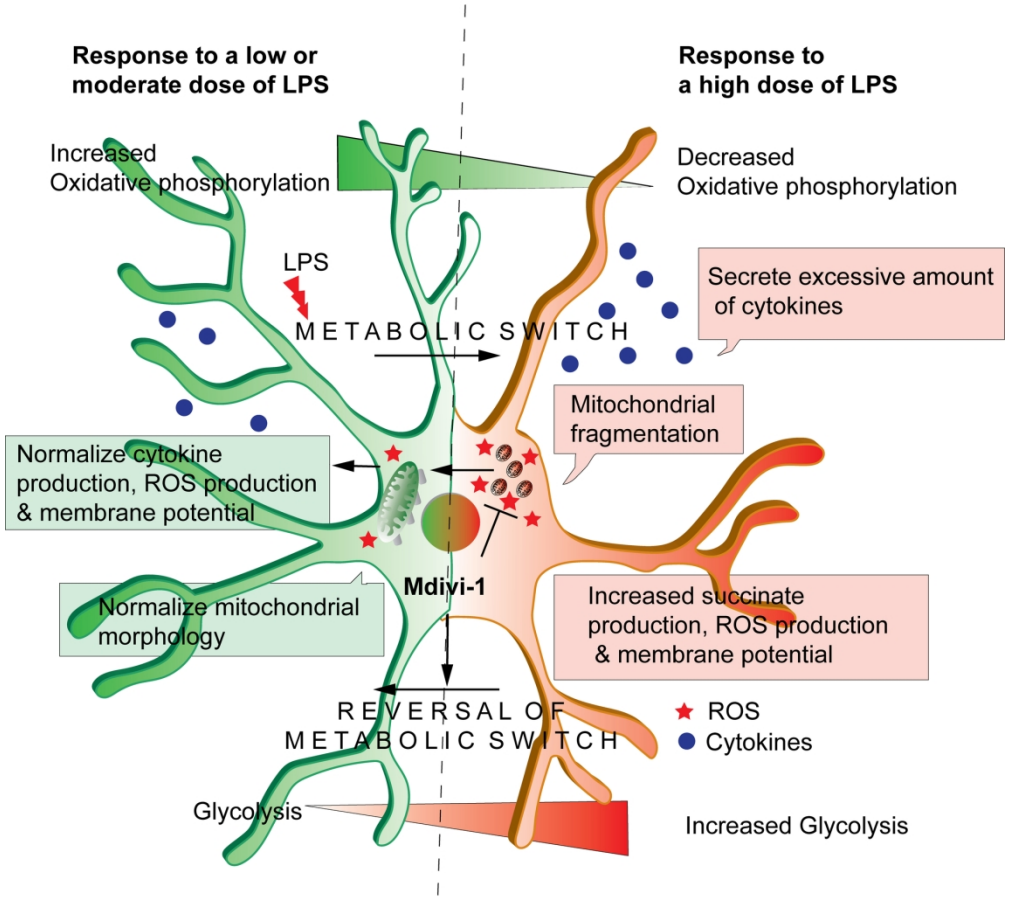

Table of Contents Image (TOCI)

173x169mm (300 x 300 DPI)

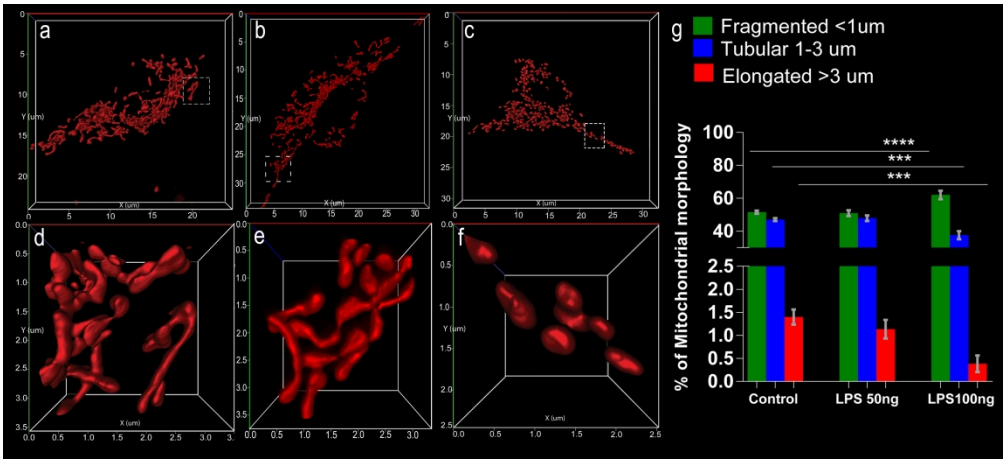

Fig:1 LPS induces dose-dependent mitochondrial fragmentation. Super-resolution microscopy reveals excessive mitochondrial fragmentation (a) Control (b) 50ng/ml LPS exposure for 24hrs (c) 100ng/ml LPS exposure for 24hrs (d-f) shows a higher magnification of the image in the white square in the upper panel. (g) Graphs showing results from an analysis of mitochondria morphology in primary microglia cells treated with LPS for 24h. The data are for at least 12 cells per condition in three independent experiments. Bar graphs expressed as mean ± SEM. ***P ≤ 0.001; student-t test calculating the difference between control and LPS treated groups.

344x157mm (300 x 300 DPI)

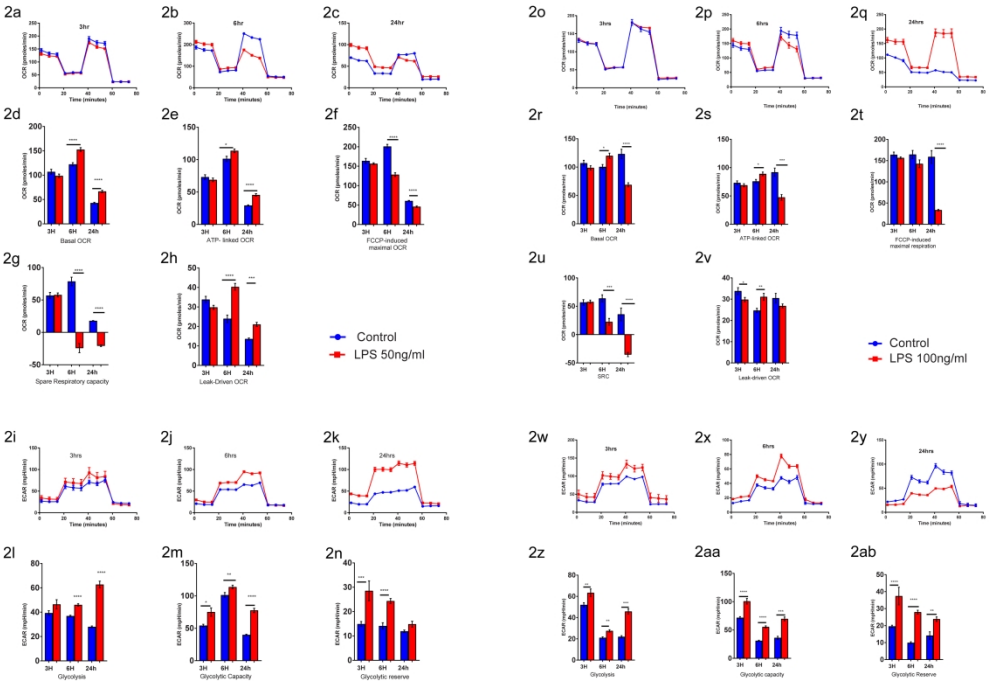

Fig:2 LPS dependent metabolic shift. Low dose of LPS (50 ng/ml) induces an increase in mitochondrial respiration and glycolysis: 50ng/ml LPS treatment shows an increase in Basal OCR, ATP linked OCR (d-e) whereas FCCP linked maximal OCR (f) and spare respiratory capacity (g) decreased from 3- 24hrs. Leak-driven OCR was also increased from 6-24hrs. Glycolytic parameters, based on ECAR, tended to increase from 3-24hrs (i-n). Whereas a high dose (100ng/ml) of LPS induces a time dependent metabolic shift. 100ng/ml LPS treatment for 6h shows an increase in Basal OCR, ATP linked OCR, while LPS treatment for 24h resulted in a decrease of Basal and ATP linked OCR (r-s). FCCP linked maximal OCR (t) and spare respiratory capacity (u) decreased from 6- 24hrs. Leak driven OCR was increased at 6 hrs (v). OCR and ECAR measured for 3,6 and 24hrs are expressed in bar graph format as the mean ± SEM n=9. *P ≤ 0.05; **P ≤ 0.01; ***P ≤ 0.001 student t test calculating the difference between control and LPS treated groups.

298x202mm (300 x 300 DPI)

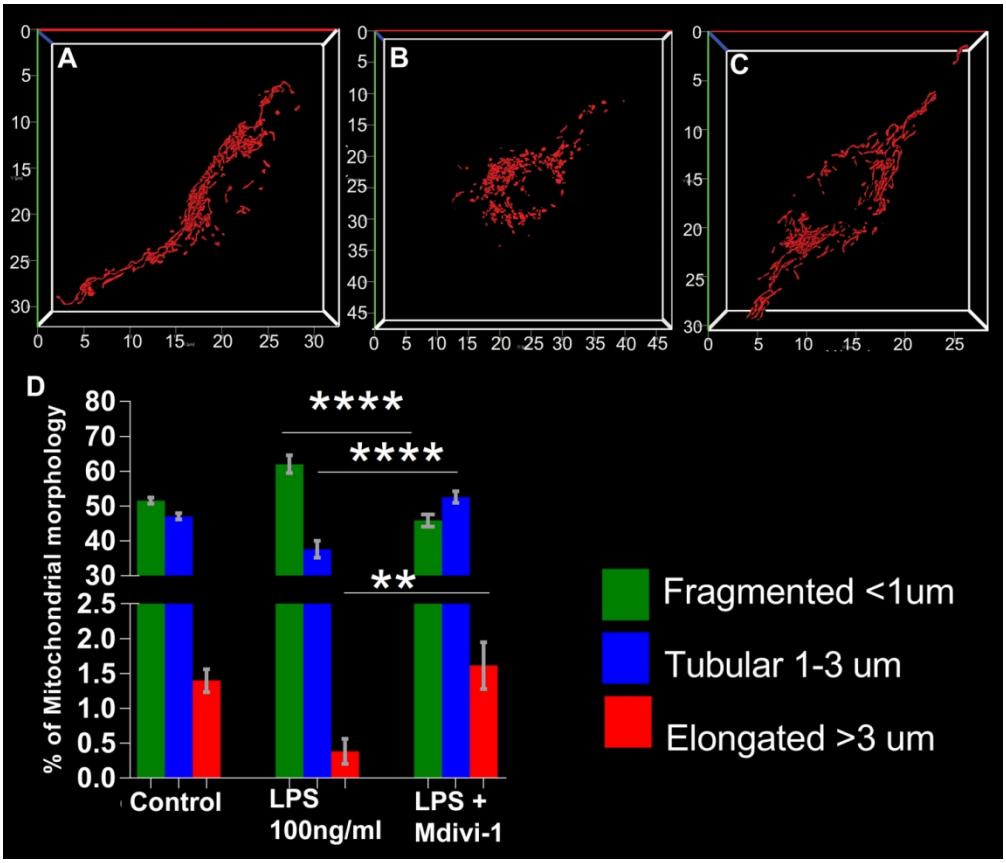

Fig.3 Pharmacologic blockade of DRP1 by Mdivi-1 re-established mitochondrial morphology. Mdivi-1 pre-treatment (25μm) for 1hr followed by LPS (100ng/ml) exposure for 24h resulted in a decrease of fragmented mitochondria and an increase in tubular and elongated mitochondria (d). A-Control cells treated with vehicle (DMSO), B- LPS (100ng/ml) exposure for 24h, C- LPS (100ng/ml)+ Mdivi-1. Bar graphs expressed as mean ± SEM. The data are for at least 12 cells per condition in three independent experiments. **P ≤ 0.01; ***P ≤ 0.001; student-t test calculating the difference between LPS and LPS+Mdivi-1 groups.

126x108mm (300 x 300 DPI)

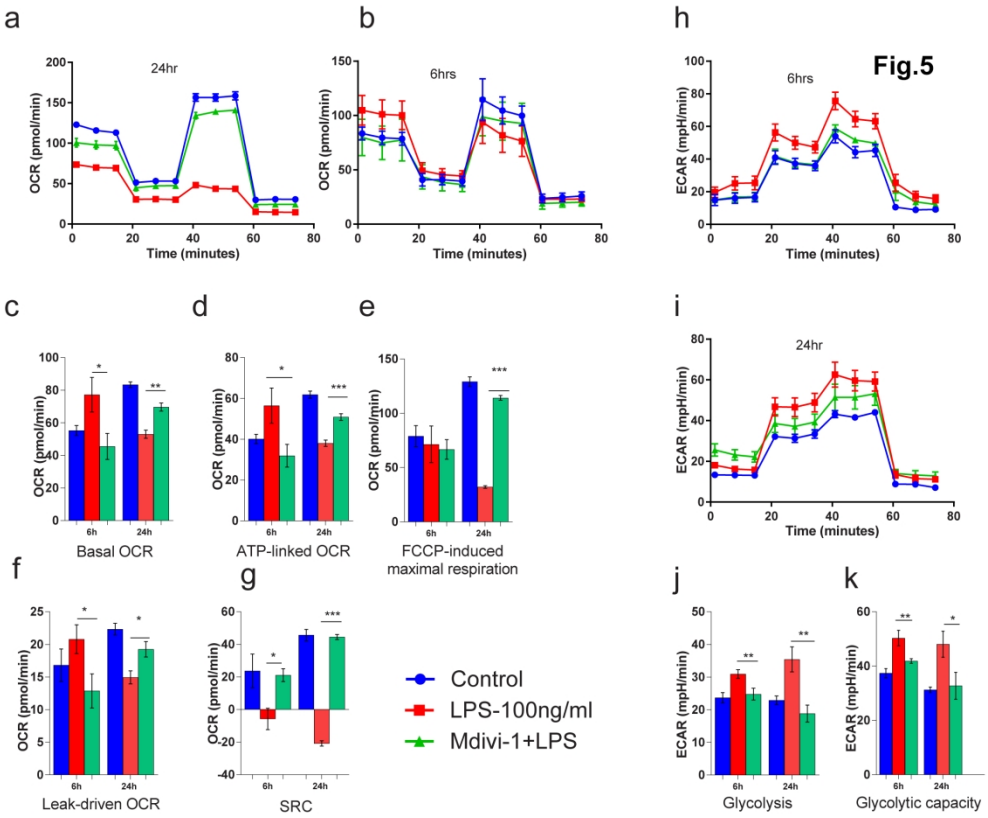

Fig.4 Mdivi-1 treatment reversed the metabolic shift. Inhibition of DRP1 by Mdivi-1 resulted in reduced basal OCR and ATP-linked OCR at 6h whereas Mdivi-1 increased basal OCR and ATP-linked OCR at 24h compared to 100ng/ml LPS exposure (c-d). LPS induced reduction in FCCP-induced maximal respiration and Leak-driven OCR at 24hr, which was normalized by Mdivi-1(e-f). The LPS-evoked drop in SRC was prevented by Mdivi-1 (g). Midivi-1 normalized LPS-induced increased ECAR dependent glycolysis and glycolytic capacity (j-h). OCR and ECAR measured for 3, 6 and 24hrs are expressed in bar graph format as the mean ± SEM n=6-9. ***P ≤ 0.001;, student-t test calculating the difference between LPS and LPS+Mdivi-1 treated groups.

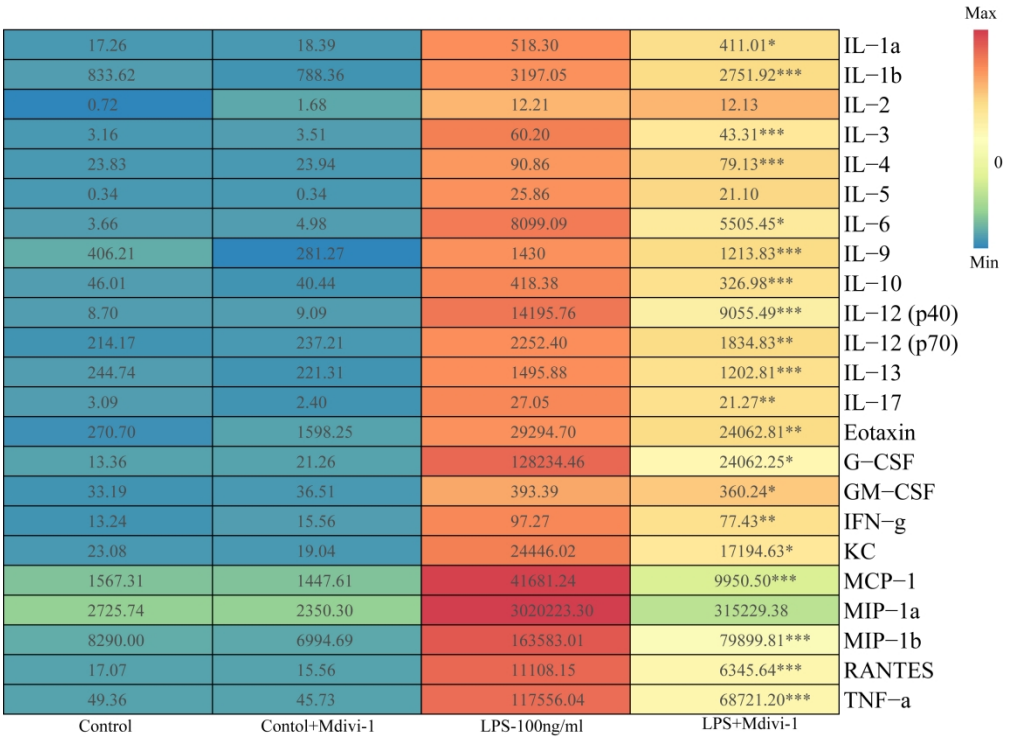

Fig.5 Mdivi-1 treatment abolished LPS induced exaggerated pro/anti cytokine and chemokine response. Microglia cells were pre-treated with Mdivi-1 (25μM) for one hour followed by LPS (100ng/ml) for 24h, MCM were collected and analysed by 23-plex cytokine assay. Heat maps show cytokine concentration (pg/ml). KC = keratinocyte chemoattractant. n=8 *P ≤ 0.05; **P ≤ 0.01; ***P ≤ 0.001;, student-t test calculating the difference between LPS and LPS+Mdivi-1 treated groups.

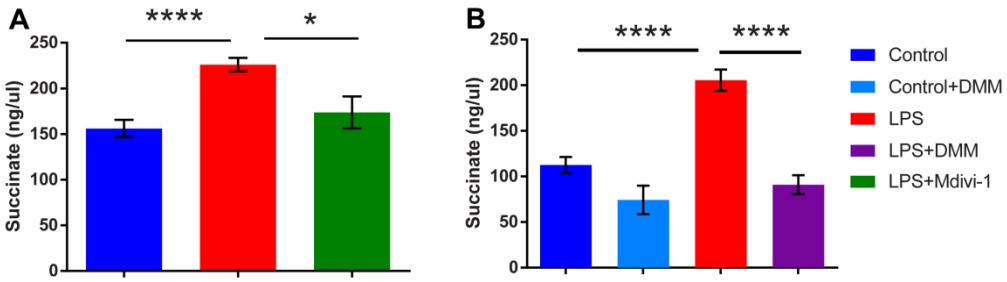

Fig.6 (A) Mdivi-1 normalized LPS induced succinate upregulation. Microglia cell homogenates of cells were analysed by succinate colorimetric assay. Microglia cells were pre-treated with Mdivi-1 (25uM; 1h) followed by LPS exposure of 100ng LPS for 24h resulted in significant downregulation of LPS induced succinate upregulation. Bar graph expressed as the mean ± SEM n=8. *P ≤ 0.05; student-t test calculating the difference between LPS and LPS+Mdivi-1 treated groups. (B) Succinate dehydrogenase inhibitor recapitulated the effects of Mdivi-1. Pre-treatment with dimethyl malonate (DMM, 10mM; 3h) prior to LPS exposure attenuated succinate accumulation. Bar graph format as the mean ± SEM n=9. *P ≤ 0.05, Turkeys post-hoc test using One-Way Anova revealed difference between control, control + DMM, LPS and LPS+DMM treated groups.

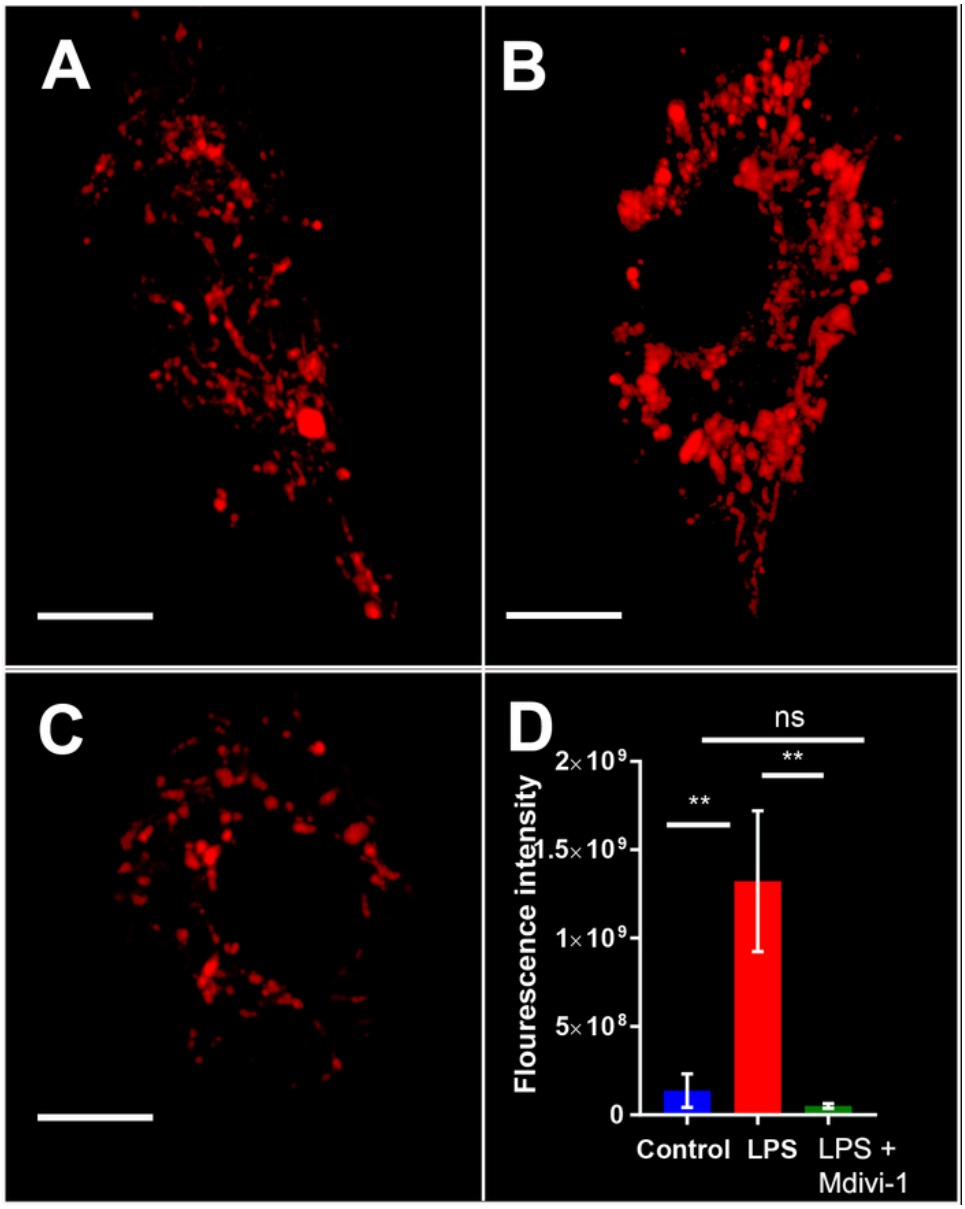

Fig.7 Mdivi-1 treatment abolished LPS induced mitochondrial ROS production. (A) Control (B) 100ng/ml LPS exposure for 24hrs (C) LPS+Mdivi-1 (D) Graphs showing results from an analysis of mitosox fluorescence by live cell airyscan microscopy. The data are for at least 12 cells per condition in three independent experiments. Bar graphs expressed as mean ± SEM. **P ≤ 0.01, student-t test calculating the difference between control LPS and Mdivi-1 treated groups.

59x74mm (300 x 300 DPI)

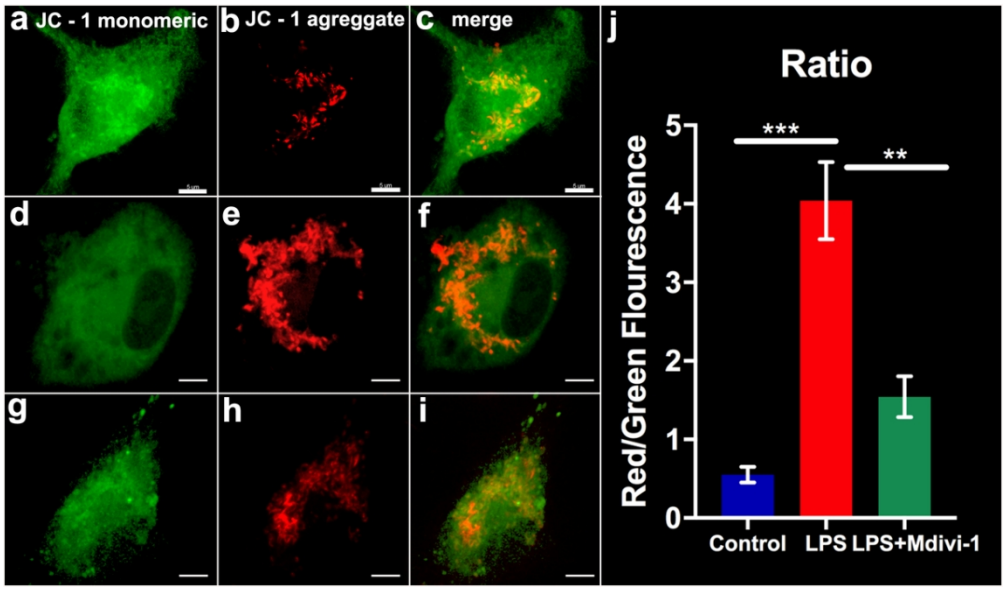

Fig.8 Mdivi-1 treatment attenuated LPS induced increase of mitochondrial membrane potential: (a-c) Control (d-e) 100ng/ml LPS exposure for 24hrs (g-h) LPS+Mdivi-1. Graphs showing results from an analysis of JC1 fluorescence 525/565 nm by live cell airyscan microscopy. The data are for at least 6 cells per condition in three independent experiments. Bar graphs expressed as mean ± SEM. **P ≤ 0.01, ***P ≤ 0.001, student-t test.

103x60mm (300 x 300 DPI)

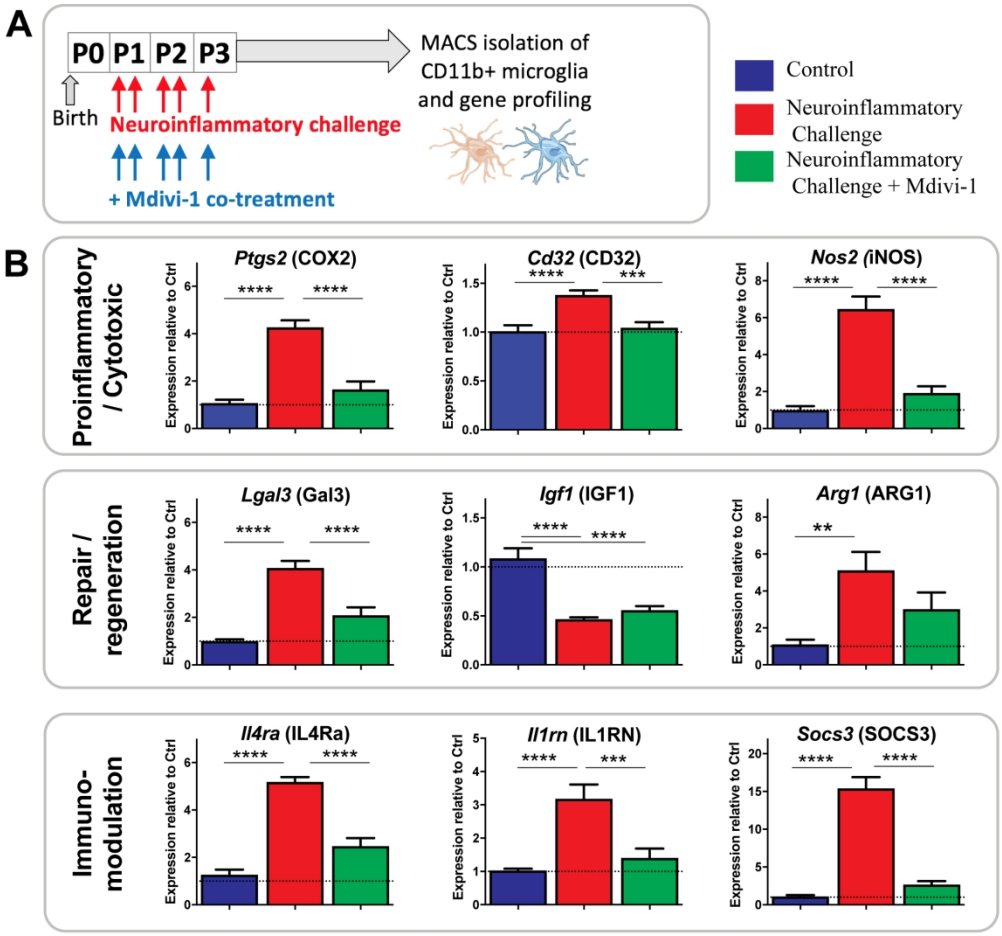

Fig.9 (A) Schematic representation of the testing of the effects of Mdivi-1 on neuroinflammation induced microglial gene expression in vivo. (B) Mdivi-1 prevented many of the neuroinflammation (IL-1β-induced) alterations in gene expression. Relative gene expression of Ptsg2, Cd32, Nos2, Lgal3, Igf1, Arg1, Il4ra, Il1rn and Socs3 were assessed by qRT-PCR from MACS isolated CD11b+ microglia from P3 mice. Protein names for the genes are shown in brackets on the panels. The legend indicates that the first bar (blue) is the control (PBS injected group), the middle bar (red) is the neuroinflammatory challenge group, and that the right bar (green) is the group challenged with neuroinflammation but also treated with Mdivi-1. The dotted line highlights the gene expression in the control group. Results are expressed as the mean ± SEM. There are 10-15 data points from three independent experiments per group. Data were analysed with a Kruskal–Wallis ANOVA, P<0.001 with a Dunn's test for comparison among groups: **p<0.01, *** p<0.001, **** p<0.0001.

190x177mm (300 x 300 DPI)

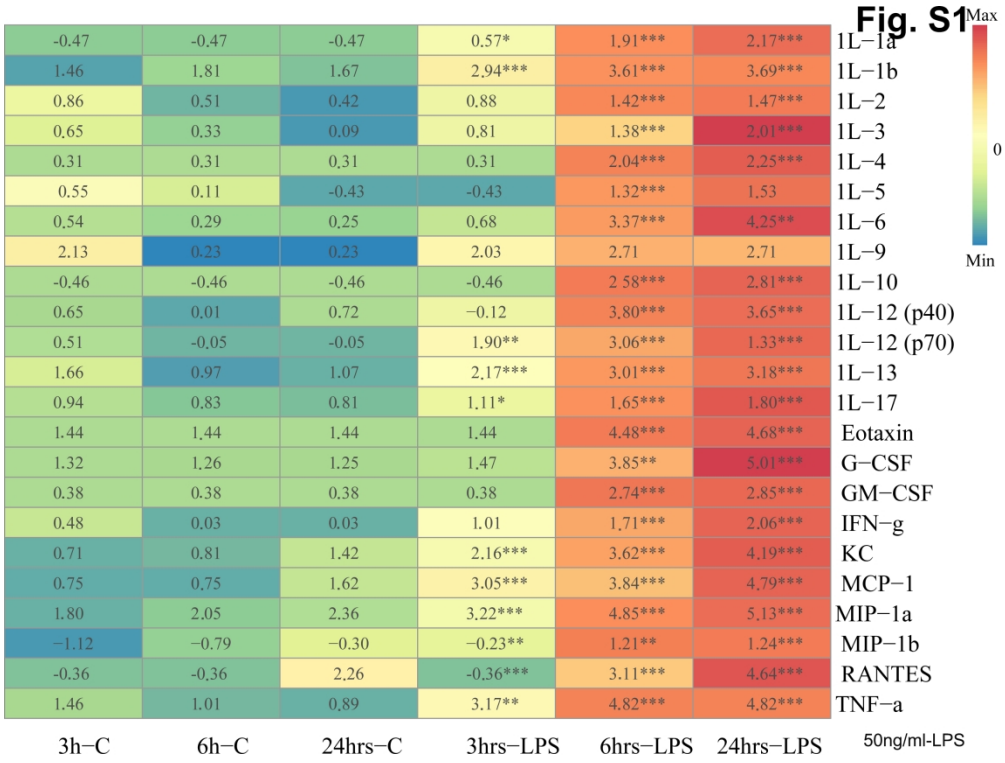

Fig. S1 and S2 (Supplementary) LPS induces exaggerated cytokine, chemokine following LPS exposure. The medium of microglial cells exposed with LPS 50 and 100ng/ml were sampled after 3,6 and 24h of LPS exposure and analyzed by 23-plex cytokine assay. Heat maps show the Log10 of cytokine concentration (pg/ml). n=8 KC = keratinocyte chemoattractant. *P ≤ 0.05; **P ≤ 0.01; ***P ≤ 0.001; student-t test calculating the difference between control and LPS treated groups.

Fig.S2

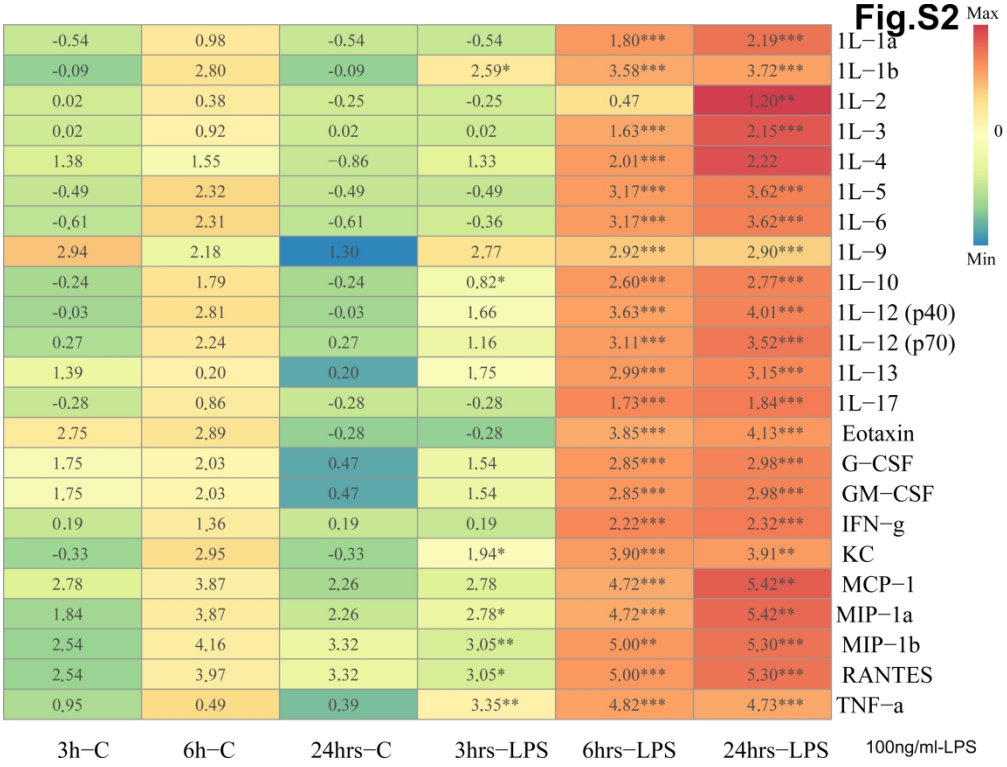
Max
0
Min
-0.54 0.98 -0.54 -0.54 1.80*** 2.19*** 1L−1a
-0.09 2.80 -0.09 2.59* 3.58*** 3.72*** 1L−1b
0.02 0.38 -0.25 -0.25 0.47 1.20** 1L−2
0.02 0.92 0.02 0.02 1.63*** 2.15*** 1L−3
1.38 1.55 −0.86 1.33 2.01*** 2.22 1L−4
-0.49 2.32 -0.49 -0.49 3.17*** 3.62*** 1L−5
-0.61 2.31 -0.61 -0.36 3.17*** 3.62*** 1L−6
2.94 2.18 1.30 2.77 2.92*** 2.90*** 1L−9
-0.24 1.79 -0.24 0.82* 2.60*** 2.77*** 1L−10
-0.03 2.81 -0.03 1.66 3.63*** 4.01*** 1L−12 (p40)
0.27 2.24 0.27 1.16 3.11*** 3.52*** 1L−12 (p70)
1.39 0.20 0.20 1.75 2.99*** 3.15*** 1L−13
-0.28 0.86 -0.28 -0.28 1.73*** 1.84*** 1L−17
2.75 2.89 -0.28 -0.28 3.85*** 4.13*** Eotaxin
1.75 2.03 0.47 1.54 2.85*** 2.98*** G−CSF
1.75 2.03 0.47 1.54 2.85*** 2.98*** GM−CSF
0.19 1.36 0.19 0.19 2.22*** 2.32*** IFN−g
-0.33 2.95 -0.33 1.94* 3.90*** 3.91** KC
2.78 3.87 2.26 2.78 4.72*** 5.42** MCP−1
1.84 3.87 2.26 2.78* 4.72*** 5.42** MIP−1a
2.54 4.16 3.32 3.05** 5.00** 5.30*** MIP−1b
2.54 3.97 3.32 3.05* 5.00*** 5.30*** RANTES
0.95 0.49 0.39 3.35** 4.82*** 4.73*** TNF−a
3h−C
6h−C
24hrs−C
3hrs−LPS
6hrs−LPS
24hrs−LPS
100ng/ml-LPS

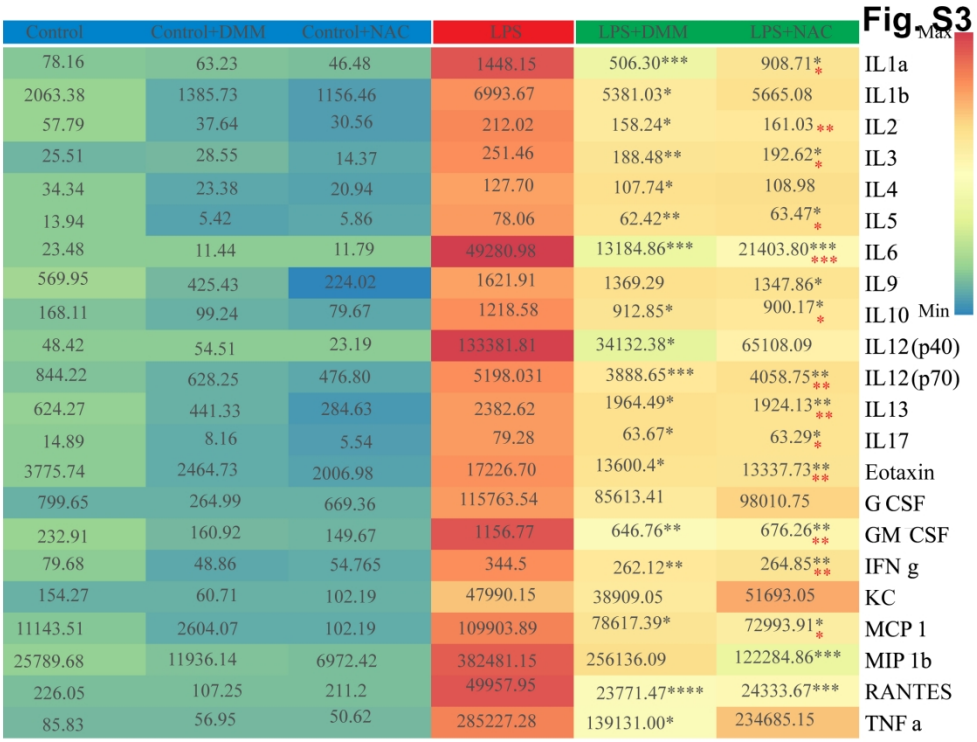

Fig.S3 (Supplementary) DMM or NAC attenuated LPS induces cytokine and chemokine production. Microglia cells were pre-treated with DMM (10mM, 3h) or NAC (10mM, 30 min) followed by LPS (100ng/ml) for 24hr, microglial culture medium was collected and analysed by 23-plex cytokine assay. Heat maps show cytokine concentration (pg/ml). KC = keratinocyte chemoattractant. n=8 *P ≤ 0.05; **P ≤ 0.01; ***P ≤ 0.001;, One-way anova and turkeys multiple test calculating the difference between Control, LPS, LPS+Mdivi-1 and LPS+NAC treated groups. *- rep significant difference with respect to LPS and treatment groups. *- rep significant difference between treatment groups

Supplementary Table 1: Primer sequences, protein targets and NCBI references

Gene	Target protein and abbreviation	Sense	Anti-sense	NCBI Reference
Inos	Inducible nitric oxide synthase (iNOS)	CCC TTC AAT GGT TGG TAC	ACA TTG ATC TCC GTG ACA	NM_010927.3
CD32	Cluster of differentiation 32 (CD32)	CTG GAA GAA GCT GCC AAA	CCA ATG CCA AGG GAG ACT AA	NM_010187.2
Ptgs2	Cyclooxygenase-2 (Cox-2)	TCA TTC ACC AGA CAG ATT	AAG CGT TTG CGG TAC TCA TT	NM_011198.3
Arg1	Arginase-1 (Arg1)	GTG AAG AAC CCA CGG TCT	GCC AGA GAT GCT TCC AAC TG	NM_007482.3
Lgals3	Galectin-3 (Gal-3)	GAT CAC AAT CAT GGG CAC	ATT GAA GCG GGG GTT AAA GT	NM_010705.3
Igf1	Insulin like growth factor 1 (IGF-1)	TGG ATG CTC TTC AGT TCG	GCA ACA CTC ATC CAC AAT GC	NM_010512.4
Il1rn	Interleukin 1 receptor antagonist (IL-1Rn)	TTG TGC CAA GTC TGG AGA	TTC TCA GAG CGG ATG AAG GT	NM_031167.5
Il4ra	Interleukin 4 receptor alpha (IL-4Rα)	GGA TAA GCA GAC CCG AAG	ACT CTG GAG AGA CTT GGT	NM_001008700.3
Socs3	Suppressor of cytokines 3 (SOCS3)	CGT TGA CAG TCT TCC GAC	TAT TCT GGG GGC GAG AAG AT	NM_007707.3